iScience

CellPress
OPEN ACCESS

Article

A role for cell polarity in lifespan and mitochondrial quality control in the budding yeast *Saccharomyces cerevisiae*

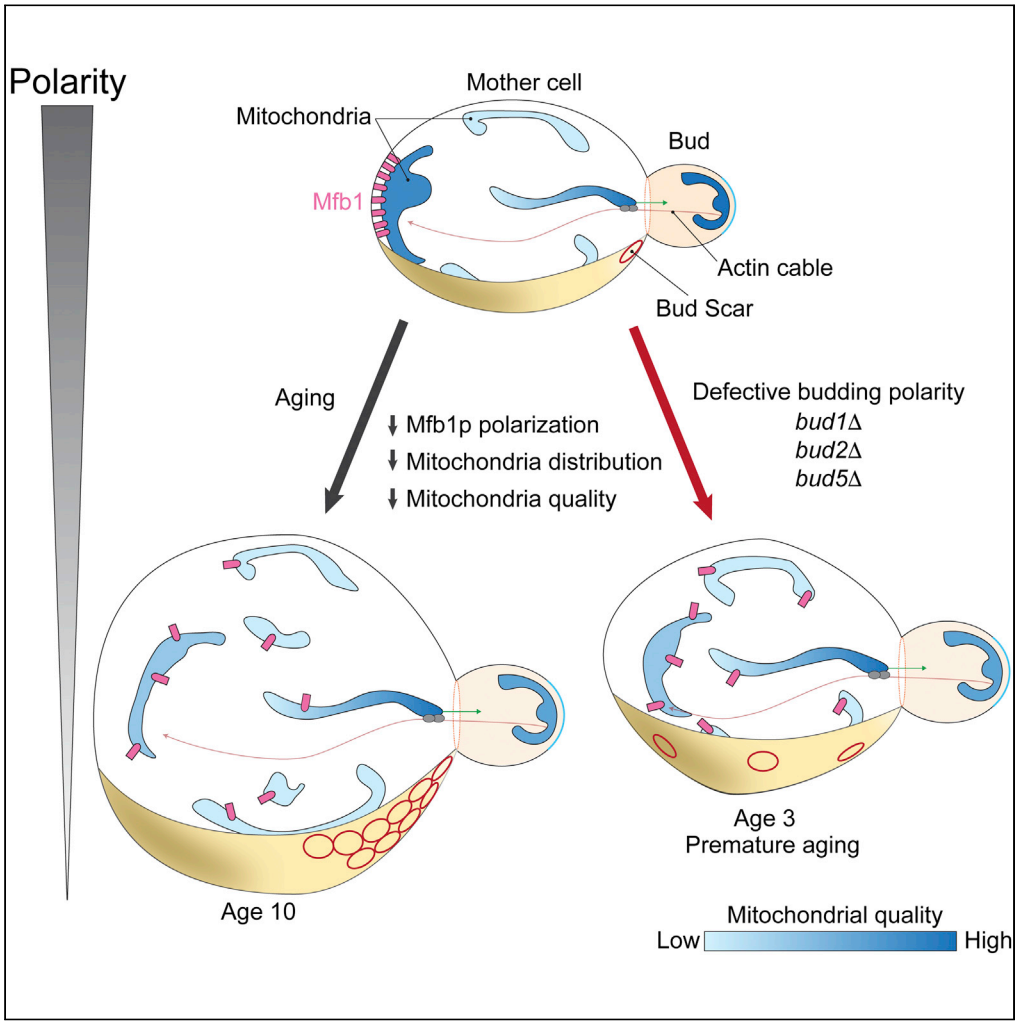

Emily J. Yang, Wolfgang M. Pernice, Liza A. Pon

lap5@cumc.columbia.edu

Highlights

Budding polarity declines with age

Polarization of a mitochondrial tether, Mfb1p, within mother cells declines with age

Defects in budding polarity disrupt Mfb1p polarization and mitochondrial distribution

Polarity defects affect Mfb1p-mediated mitochondrial quality and lifespan control

Yang et al., iScience *25*, 103957
March 18, 2022
https://doi.org/10.1016/j.isci.2022.103957

iScience

CellPress
OPEN ACCESS

Article

A role for cell polarity in lifespan and mitochondrial quality control in the budding yeast *Saccharomyces cerevisiae*

Emily J. Yang,[1,3] Wolfgang M. Pernice,[1,2,3] and Liza A. Pon[1,4,*]

SUMMARY

Babies are born young, largely independent of the age of their mothers. Mother-daughter age asymmetry in yeast is achieved, in part, by inheritance of higher-functioning mitochondria by buds and retention of some high-functioning mitochondria in mother cells. The mitochondrial F box protein, Mfb1p, tethers mitochondria at both poles in a cell cycle-regulated manner: it localizes to and anchors mitochondria at the mother cell tip throughout the cell cycle and at the bud tip before cytokinesis. Here, we report that cell polarity and polarized localization of Mfb1p decline with age in *Saccharomyces cerevisiae*. Moreover, deletion of genes (*BUD1*, *BUD2*, and *BUD5*) that mediate symmetry breaking during establishment of cell polarity and asymmetric yeast cell division cause depolarized Mfb1p localization and defects in mitochondrial distribution and quality control. Our results support a role for the polarity machinery in lifespan through modulating Mfb1 function in asymmetric inheritance of mitochondria during yeast cell division.

INTRODUCTION

Mitochondria are cell fate determinants that are differentially segregated during asymmetric cell division in stem cells and budding yeast. Indeed, new and old mitochondria are segregated during division of human mammary stem-like cells. The daughter cell that preferentially inherits new mitochondria retains stem cell properties, whereas the daughter that inherits old mitochondria becomes a tissue progenitor cell (Katajisto et al., 2015). Similarly, in the budding yeast, *Saccharomyces cerevisiae*, the daughter cell or bud inherits fitter mitochondria that are more reduced, have lower reactive oxygen species levels (ROS), and higher membrane potential ($\Delta\psi$). This in turn, allows daughter cells to live a full lifespan, whereas mother cells, which inherit lower-functioning mitochondria, continue to age (Higuchi et al., 2013; McFaline-Figueroa et al., 2011).

Three critical events occur during asymmetric cell division: breaking of cellular symmetry, polarity establishment and maintenance to generate anterior and posterior poles, and polarized cell division (Rose and Gönczy, 2014). In yeast, bud site selection, determining the site for the formation of daughter cells or buds on mother cells, is one hallmark of cell symmetry breaking. Bud site selection is controlled by a system of polarity cues and culminates in the activation of Bud1p/Rsr1p, a Ras-like GTPase, at the selected bud site (Bender and Pringle, 1989). The activity of Bud1p is tightly controlled: it is activated by *BUD5*, the guanine nucleotide exchange factor (GEF), and quickly inactivated by *BUD2*, the GTPase-activating protein (GAP) (Bender, 1993; Chant et al., 1991; Chant and Herskowitz, 1991; Kang et al., 2001; Park et al., 1993, 1999; Powers et al., 1991).

These bud site selection proteins promote polarization of the cytoskeleton toward the selected bud site. Bud1p/Rsr1p that is activated at the selected bud site recruits Cdc24p to that site (Zheng et al., 1995). This, in turn, results in region-specific activation of Cdc42p, Cdc42p-dependent assembly of actin cables at that site, and actin cable-driven transport of all cellular constituents toward the selected bud site leading to bud formation and growth (Fehrenbacher et al., 2004; Moseley and Goode, 2006). Polarized actin cables also transport and further enrich Cdc42p at the bud tip (Slaughter et al., 2009). Finally, actin cables enable segregation of mitochondria in dividing yeast by mediating 1) preferential transport of higher-functioning mitochondria from the mother cell to bud (Higuchi et al., 2013) and 2) transport of one of the tethers

[1]Department of Pathology and Cell Biology, Columbia University, New York, NY 10032, USA

[2]Present address: Department of Neurology, Columbia University, New York, NY 10032

[3]These authors contributed equally

[4]Lead contact

*Correspondence: lap5@cumc.columbia.edu

https://doi.org/10.1016/j.isci.2022.103957

(Mmr1p) that anchors and retains those higher-functioning mitochondria at the bud tip (Shepard et al., 2003; Swayne et al., 2011). Indeed, promoting actin cable function in asymmetric mitochondrial inheritance during cell division promotes daughter cell fitness and extends lifespan in yeast (Higuchi et al., 2013).

Interestingly, although the bud site selection machinery acts to break cell symmetry at a specific site on the yeast cell surface and to maintain a stable mother-to-bud axis between cell divisions (Bi and Park, 2012; Slaughter et al., 2009; Wu and Lew, 2013), it is not essential for polarized cell division in yeast per se (Kozubowski et al., 2008). In the absence of *BUD1/RSR1*, polarity factors cluster at multiple, seemingly random sites throughout the mother-cell cortex at the onset of cell division. This leads to a competition between different sites, and ultimately, to establishment of polarity at a single site followed by polarized yeast cell division (Wu et al., 2013).

Nonetheless, the bud site machinery is critical for lifespan control in yeast: loss of *BUD1* and polarity cue-guided bud site selection reduces replicative lifespan (RLS) (Clay et al., 2014) and chronological lifespan (Campos et al., 2018). These studies also revealed that *BUD1/RSR1* is required for establishing a diffusion barrier in the ER at the bud neck, which promotes retention of oxidatively damaged ER proteins in the mother cell (Clay et al., 2014). Because asymmetric inheritance of oxidized proteins is critical for normal RLS, the bud site selection machinery may contribute to RLS through its function in the ER diffusion barrier at the bud neck. However, deletion of *BUD1* actually extends RLS in yeast exposed to ER stress (Clay et al., 2014). Thus, the reduced lifespan observed upon deletion of *BUD1* is not because of effects on the diffusion barrier in the ER at the bud neck.

Moreover, although the bud tip is well established as the anterior pole in asymmetrically dividing yeast, with distinctive membrane, organelle, mRNA, and protein constituents, emerging evidence indicates that the tip of the mother cell that is distal to the bud may be the posterior pole. Specifically, a small population of mitochondria that are higher functioning compared to other mitochondria in the mother cell, are anchored at and accumulate in the mother cell tip (Pernice et al., 2016; Yang et al., 1999). This process is critical for mitochondrial quality control, yeast cell fitness and lifespan, and mother-daughter age asymmetry (Pernice et al., 2016; Yang et al., 1999).

Mfb1p, a mitochondria-associated F-box protein (Dürr et al., 2006; Kondo-Okamoto et al., 2006), serves as a tether to anchor higher-functioning mitochondria in the mother cell tip (Pernice et al., 2016). Mfb1p localization and function are polarized at two levels (Pernice et al., 2016). First, Mfb1p is asymmetrically distributed between mother and daughter cells. Through most of the cell cycle, Mfb1p is excluded from the daughter cell. That is, it localizes to mitochondria exclusively in the mother cell. However, shortly before cytokinesis, some Mfb1p localizes to mitochondria in the bud. Second, Mfb1p exhibits polarized localization within the mother cell: it localizes solely to mitochondria that accumulate at the mother cell tip. Indeed, Mfb1p is the only known protein that localizes to the mother cell tip through the entire cell cycle.

Finally, Mfb1p functions in mitochondrial distribution and quality control. Specifically, it functions to tether mitochondria in the mother cell tip throughout the cell cycle and contributes to anchorage of mitochondria in the bud tip after cytokinesis. Importantly, the mitochondria that are tethered at the mother cell tip and bud tip are more reduced and therefore higher functioning compared to other mitochondria in the yeast cell. Mfb1p function in mitochondrial distribution and quality control contributes to lifespan control in yeast: deletion of *MFB1* results in defects in anchorage of mitochondria in the mother cell tip, reduced mitochondrial function throughout the cell, and premature aging (Pernice et al., 2016).

Here, we tested whether the bud site selection machinery is critical for Mfb1p localization and function in mitochondria distribution and function, and how this contributes to lifespan. We provide evidence that the fidelity of bud site selection and the polarized localization of Mfb1p decline early in the aging process in budding yeast. We also identify a role for the bud site selection machinery in lifespan and mitochondrial quality control through effects on the polarized localization of Mfb1p at the distal tip of the yeast mother cell.

RESULTS

Budding polarity declines with age

One model for the aging process in yeast is replicative lifespan (RLS), a measure of the number of times that a mother cell can divide before senescence (Longo et al., 2012). Although yeast strains can undergo up to

35–45 generations of replicative aging, age-associated phenotypes are evident at earlier replicative ages. Indeed, mitochondrial redox state begins to decline in yeast that have undergone five rounds of cell division (age 5) (McFaline-Figueroa et al., 2011). Similarly, decreases in the acidification of the yeast cell and vacuole (the lysosome of yeast) are evident at age 4 (Henderson et al., 2014; Hughes and Gottschling, 2012). Finally, an increase in DNA damage, which is detected by an increase in foci containing the DNA repair protein Rad52p in the yeast nucleus, is detected at age 7 (Alvaro et al., 2007; Novarina et al., 2017). These findings raise the possibility that changes which occur early during the yeast RLS may cause or contribute to the aging process.

Here, we studied whether bud site selection changes during aging. Yeast cells of defined replicative age were isolated using a miniature chemostat aging device (mCAD) (Hendrickson et al., 2018). Mid-log phase yeast, which are largely young cells, were immobilized and allowed to undergo replicative aging in the mCAD (Figure 1A). Daughter cells produced from immobilized cells were removed by continuous media exchange, and yeast of defined replicative age were harvested from the mCAD. We confirmed the efficacy of the mCAD for these studies: immobilized cells isolated from mCAD exhibit increasing age and aging phenotypes, including an increase in cell size and a decrease in viability, as a function of the time of propagation in mCAD (Figures 1B and S1A–S1C).

The bud scar is a chitinous ring on the cell wall of the mother cell that forms where buds separate from mother cells. It serves as a marker for the number of times a mother cell divides and as a landmark for cell symmetry breaking during establishment of cell polarity. In haploid yeast cells that undergo axial or unipolar budding, new bud sites form adjacent to the bud site from the previous round of cell division, which is marked by the bud scar (Chant and Pringle, 1995).

To assess the fidelity of axial budding, bud scars were visualized using wheat germ agglutinin (WGA), a chitin-binding agent. Inspired by TrackScar (Maxwell and Magwene, 2017), we sequentially stained yeast bud scars with WGA conjugated to different fluorescent dyes to distinguish new from old bud scars. Cells were first stained with Alexa 488-WGA to label all bud scars. They were then propagated for 2 h and stained with Alexa 594-WGA to label the two newest bud scars (Figure 1A). Here, bud site selection was scored as polarized if the two newest bud scars were adjacent to each other and random if those bud scars were not adjacent.

We found that bud site selection is polarized in >97% of the young cells (1-4 generations) examined. However, loss of budding polarity is evident early in the aging process. Random bud site selection was detected in 11.0% of aged cells at age 6–10 in RLS and increased further to 27.7 and 30.6% in cells of more advanced age, 11–20 and >20 generations, respectively (Figures 1C and 1D). Thus, polarity establishment during bud site selection declines with age in yeast and these declines are evident early in the aging process. Interestingly, the proportion of cells displaying randomized bud-site selection plateaus at ca. 30% for cells of age 11–20 and beyond.

Polarization of Mfb1p within mother cells but not between mother cells and buds declines with age

Next, we tested whether aging affects the function and polarized localization of Mfb1p. We visualized mitochondria and Mfb1p using Cit1p-mCherry (a mitochondrial matrix marker) and Mfb1p-GFPEnvy, respectively, in yeast of defined replicative age. Because Mfb1p localizes to the mother cell throughout the cell cycle and to the bud tip late in the cell division cycle, we restricted analysis to cells in early stages of the cell cycle (bud-to-mother ratios between 0.2 and 0.6) when Mfb1p localizes exclusively to the mother tip.

We detect co-localization of Mfb1p with mitochondria throughout the aging process in yeast (Figure 2A). Quantitative analyses of co-localization of Mfb1p with mitochondria using Pearson's coefficient and Manders' M1 coefficient indicate that there is no significant difference in the co-occurrence of Mfb1p with mitochondria as a function of replicative age (Figures S2A and S2B). Interestingly, Manders' M2 coefficient, a measure of co-localization of mitochondria with Mfb1p, gradually increases with age.

In contrast, we find that the polarized localization of Mfb1p within mother cells declines with age (Figures 2A and 2B). Moreover, this decline is evident early in the aging process. We confirmed that Mfb1p co-localizes with mitochondria exclusively at the distal tip of young mother cells (1-4 generations), which reflects

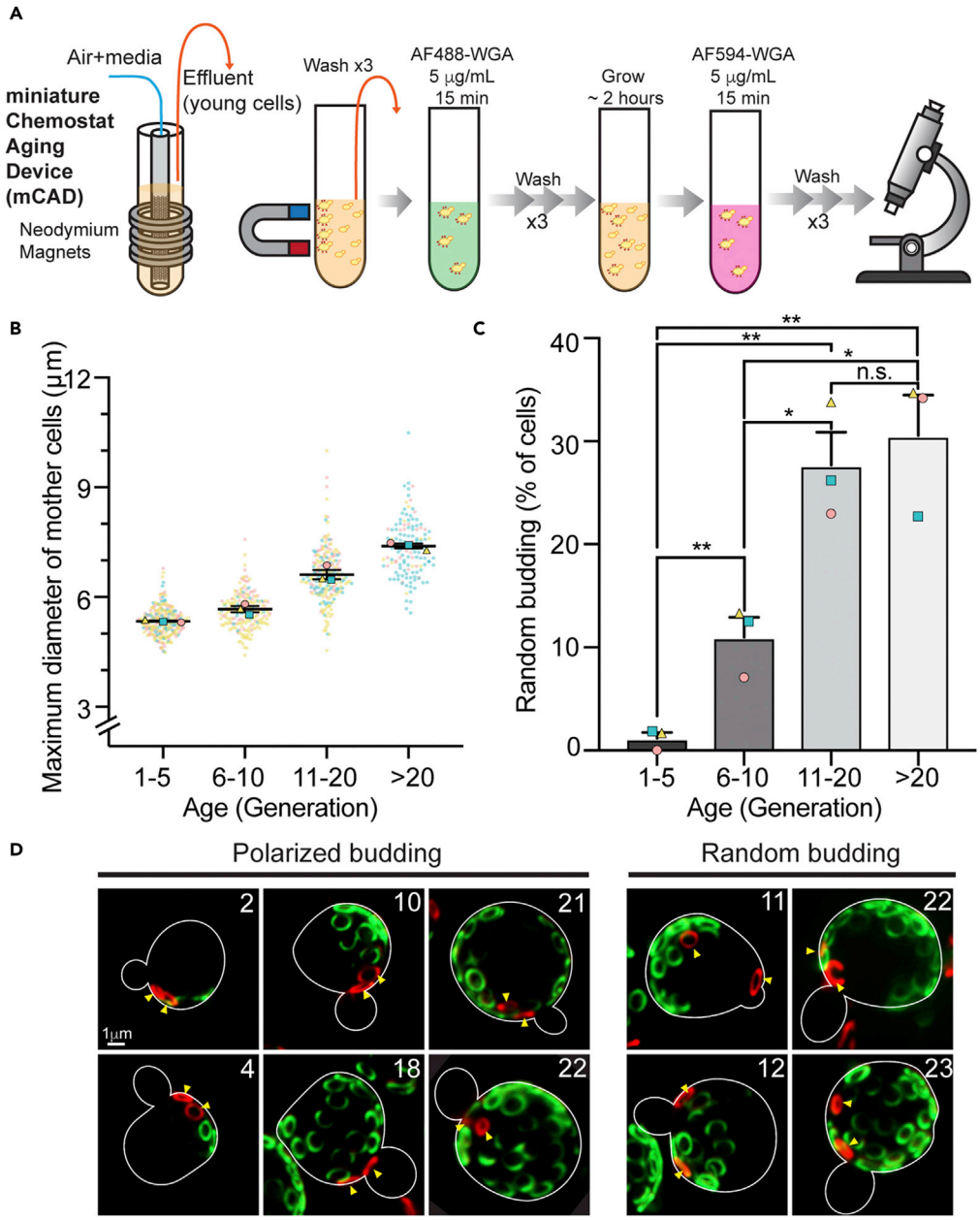

Figure 1. Polarized bud site selection declines as yeast cells age

(A) Illustrations of the miniature chemostat aging device (mCAD) used to isolate cells of different replicative age (left) and the approach used to monitor budding polarity with age by labeling older bud scars with Alexa 488-WGA and the two newest bud scars with Alexa 594-WGA (right).

(B) Quantification of cell diameter as a function of time of propagation in the mCAD and replicative age. The diameter measured was the longest axis of the mother cell. Data are represented as mean ± SEM.

(C) Quantification of percentage of cells with random bud site selection. Data are represented as mean ± SEM, n = 3 independent trials. n >50 cells/age group/trial. The unpaired two-tailed t test was used for statistical analysis. p values are denoted as: **p <0.01; *p <0.05.

(D) Representative images of the budding pattern of cells of different replicative age. Replicative age (number in right corner of each image) was determined by scoring the number of WGA-stained bud scars. Older bud scars were labeled with Alexa 488-WGA (green). Yellow arrowheads: new Alexa 594-WGA-stained bud scars (red).

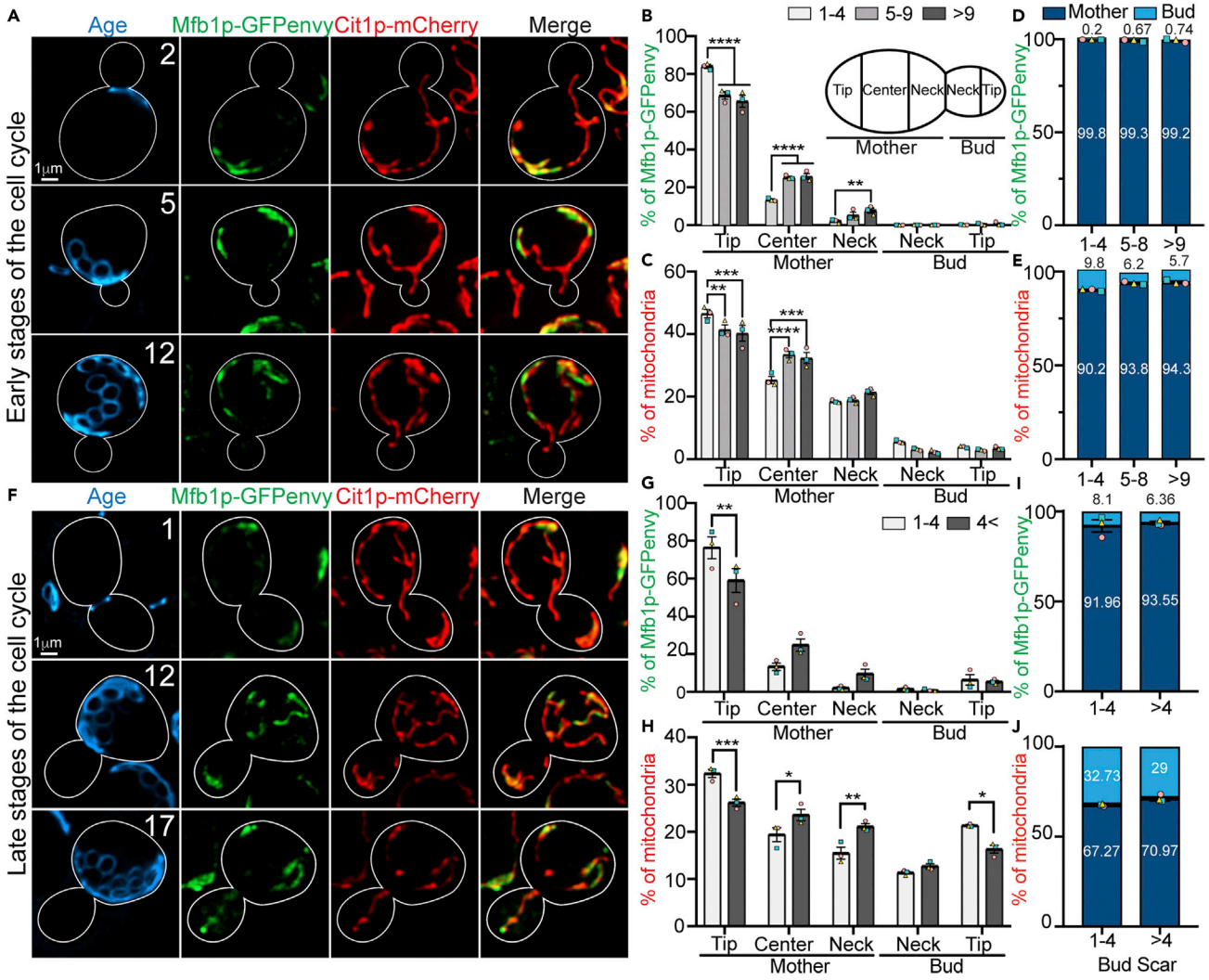

Figure 2. Polarized distribution of Mfb1p and mitochondria within the yeast mother cell but not between mother cells and buds declines with age

Age-associated changes early in the cell cycle

(A) The localization of Mfb1p and mitochondria in cells during early stages in the cell cycle as a function of replicative age. Mitochondria and Mfb1p were visualized by tagging the mitochondrial marker protein Cit1p with mCherry (red) and Mfb1p with GFP (green). To visualize cells early cell cycle stages, cells with mother:bud ratio of 0.2–0.6 were analyzed. The replicative age was determined by scoring calcofluor white-stained bud scars (blue). Cells were grouped according to age: 1–4, 5-9, and >9 generations (n >49, 72, and 31 cells, respectively, in three independent trials). Images shown are maximum projections. Cell outlines: white. Scale bars: 1 μm.

(B and C) Quantification of the distribution of Mfb1p and mitochondria by measurement of the integrated fluorescence in five regions of interest (ROIs) defined at the upper right panel. (B) Data are represented as mean ± SEM, p <0.0001 (one-way ANOVA with Tukey's multiple comparisons test).

(D and E) Quantification of the integrated fluorescence of Mfb1p and mitochondria in mother cells and buds. Data are represented as mean ± SEM. (D) p <0.3312 (one-way ANOVA with Tukey's multiple comparisons test). (E) p <0.0001 (one-way ANOVA with Tukey's multiple comparisons test).

(F-J) Age-associated changes late in the cell cycle.

(F) The localization of Mfb1p and mitochondria in cells during late stages in the cell cycle as a function of replicative age as carried out as for panel. (A) Cells with mother:bud ratios of 0.6–0.8 were grouped according to age: 1-4 and >4 generations (n >33 and 46 cells, in three independent trials).

(G–J) Quantification of the integrated fluorescence of Mfb1p and mitochondria in five ROIs (G and H) and in mother cells and buds (I and J). Data are represented as mean ± SEM, p values are denoted as: ****p <0.0001; ***p <0.001; **p <0.01; *p <0.05. (G) p <0.0024 (one-way ANOVA with Tukey's multiple comparisons test). (H) p <0.0001 (one-way ANOVA with Tukey's multiple comparisons test).

Mfb1p function as a tether for mitochondria in the mother distal tip. However, we detect a decrease in the amount of Mfb1p-GFPEnvy and mitochondria in the mother distal tip and a corresponding increase in Mfb1p-GFPEnvy and mitochondrial levels in the center of the mother cell early during the aging process (age 5–9) (Figures 2B and 2C).

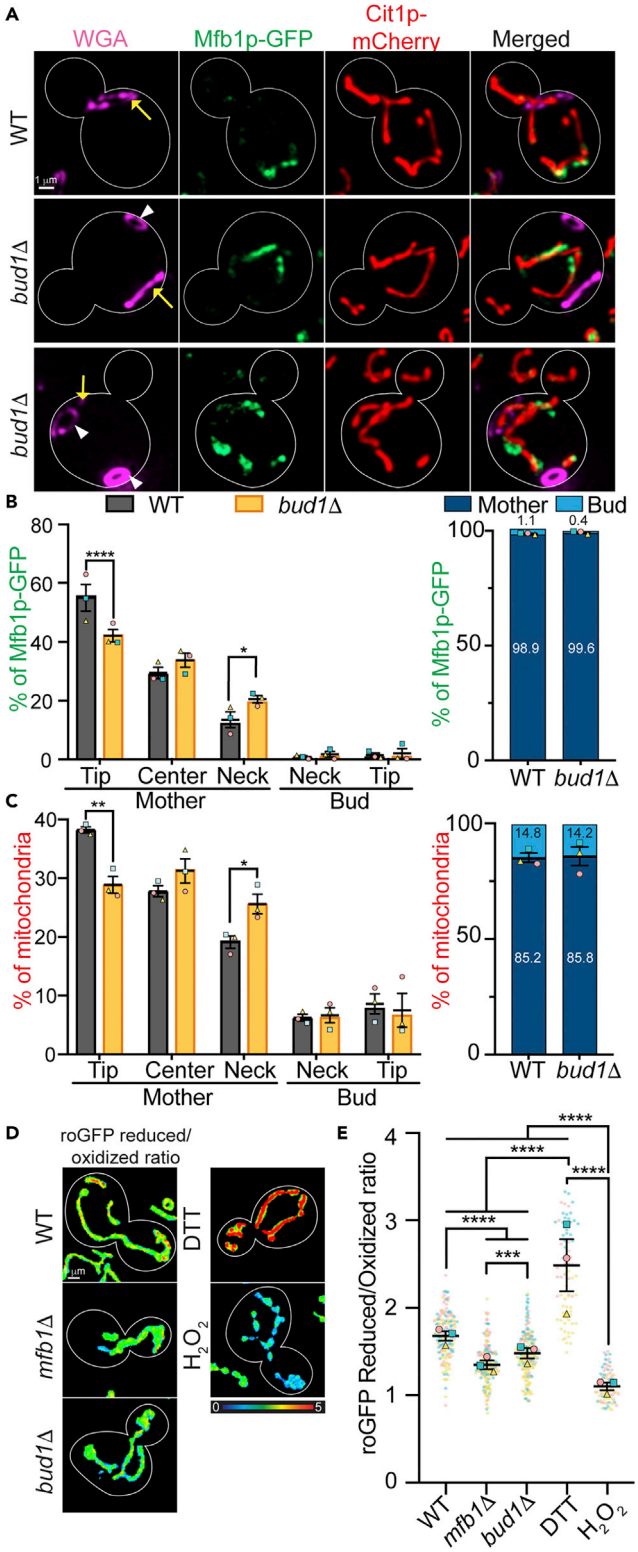
A
WGA
Mfb1p-GFP
Cit1p-mCherry
Merged
WT
bud1Δ
bud1Δ
1 μm
B
WT
bud1Δ
Mother
Bud
% of Mfb1p-GFP
Tip
Center
Neck
Neck
Tip
Mother
Bud
1.1
0.4
98.9
99.6
WT
bud1Δ
C
% of mitochondria
14.8
14.2
85.2
85.8
D
roGFP reduced/oxidized ratio
WT
mfb1Δ
bud1Δ
DTT
H2O2
E
roGFP Reduced/Oxidized ratio
WT
mfb1Δ
bud1Δ
DTT
H2O2

Figure 3. Deletion of *BUD1* results in depolarized localization of Mfb1p, defects in mitochondrial distribution, decreased mitochondrial quality, and reduced RLS

(A) Representative maximum projection images of Mfb1p (green) and mitochondria (red) in mid-log phase WT or *bud1*Δ cells visualized as for Figure 2A. The budding pattern was determined by staining birth and bud scars with Alexa 647-WGA. Cell outlines: white. Yellow arrows: birth scars. White arrowheads: bud scars. Scale bars: 1 μm.

(B and C) ROIs are defined as for Figure 2B. n >60 cells/strain/trial. Data are represented as mean ± SEM. The mean of three independent trials is shown with differently shaped and colored symbols for each trial. p <0.0003 (one-way ANOVA with Tukey's multiple comparisons test). p values are denoted as: ****p <0.0001; ***p <0.001; **p <0.01; *p <0.05. (B and C) Relative distribution of Mfb1p-GFP and mitochondria in WT and *bud1*Δ cells at specific regions within the cell (left panels) or in mother cells and buds (right panels).

(D) Maximum projections of ratiometric images of reduced/oxidized integrated mito-roGFP1 in mid-log phase WT, *mfb1*Δ, and *bud1*Δ cells. DTT and H_2O_2 treated WT cells were controls and illustrate the dynamic range of mito-roGFP1. Colors reflect the intensity of the ratio of reduced-to-oxidized mito-roGFP1 (scale at the bottom). Cell outlines: white. n >170 cells.

(E) Quantification of reduced/oxidized mito-roGFP1 of mitochondria in mother cells of genotypes or treatments shown in (D). The means of three independent trials are shown, with differently shaped and colored symbols for each trial. Mean ± SEM of the ratio of reduced/oxidized mito-roGFP1: 1.678 ± 0.0544 (WT), 1.349 ± 0.0495 (*mfb1*Δ), 1.480 ± 0.06 (*bud1*Δ), 2.486 ± 0.298 (DTT), 1.103 ± 0.0438 (H_2O_2). p <0.0001 (one-way ANOVA with Tukey's multiple comparisons test). p values are denoted as: ****p <0.0001; ***p <0.001; **p <0.01; *p <0.05.

Interestingly, the age-associated decline in localization of Mfb1p to mitochondria in the mother cell tip results in relocalization to mitochondria at other regions within the mother cell, but not to mitochondria in the bud (Figures 2A, 2C, and 2E). Thus, asymmetric distribution of Mfb1p between mother cells and buds appears to persist with age. To test this hypothesis, we studied the localization of Mfb1p late in the cell cycle, when some Mfb1p localizes to the bud where it contributes to anchorage of mitochondria at that site (Figures 2F–2J). Age-associated declines in polarization of Mfb1p and mitochondria within mother cells are evident at late stages in the cell cycle. Mfb1p localizes exclusively to mitochondria that accumulate in the mother cell tip at age 1-4 in yeast bearing large buds. However, at age >4, some Mfb1p is detected at mitochondria throughout the mother cell (Figures 2F–2G). Interestingly, we detect accumulation of Mfb1p and mitochondria in the bud tip in young and old yeast late in the cell division cycle. Indeed, there is no significant change in the amount of Mfb1p that localizes to mitochondria in the bud tip during the aging process (Figures 2F–2I). There is a subtle but significant decrease in accumulation of mitochondria with age (Figures 2F, 2H, and 2J). Because Mfb1p contributes to but is not solely responsible for tethering mitochondria at the bud tip late in the cell cycle (Pernice et al., 2016), it is not clear whether those changes are because of effects on Mfb1p. Overall, our findings support the model that Mfb1p is polarized both within mother cells and between mother cells and buds, and that only the former, localization of Mfb1p to mitochondria in the mother cell tip, declines with replicative age, and does so early in the aging process.

Disabling bud site selection machinery disrupts the polarized localization and function of Mfb1p in the mother cell tip but not Mfb1p asymmetric localization between mother cells and buds

To determine whether the age-linked declines in Mfb1p are because of changes in the bud site selection machinery, we monitored Mfb1p distribution and function in yeast bearing a deletion in *BUD1*. We confirmed that deletion of *BUD1* results in random bud site selection in haploid yeast cells. On the other hand, deletion of *MFB1* does not affect bud site selection (Figures S3A–S3B).

Next, we quantified the distribution of Mfb1p-GFP and mitochondria in WT and *bud1*Δ mutant cells. Interestingly, deletion of *BUD1* produces defects in Mfb1p localization and function that are similar to those produced early in the aging process. Deletion of *BUD1* has no obvious effect on 1) the steady-state level of Mfb1p (data not shown), 2) association of Mfb1p with mitochondria (Figure S4), 3) inheritance of mitochondria by yeast daughter cells, or 4) the asymmetric distribution of Mfb1p between mother cells and buds (Figures 3A–3C, right panels). However, loss of axial bud site selection interferes with the polarization of Mfb1p and mitochondria within mother cells (Figures 3A–3C, left panels). Specifically, deletion of *BUD1* results in a decrease in the accumulation of Mfb1p and mitochondria at the mother cell tip, and a compensatory shift of Mfb1p and mitochondrial mass to the mother cell neck in mid-log phase cultures. Thus, Mfb1p relocalizes to mitochondria in the mother cell but not in the bud in *bud1*Δ cells. Interestingly, the defects in accumulation of mitochondria in the mother cell tip in *bud1*Δ cells are not as severe as those observed upon deletion of *MFB1*. As such, our findings indicate that the accumulation of Mfb1p and its

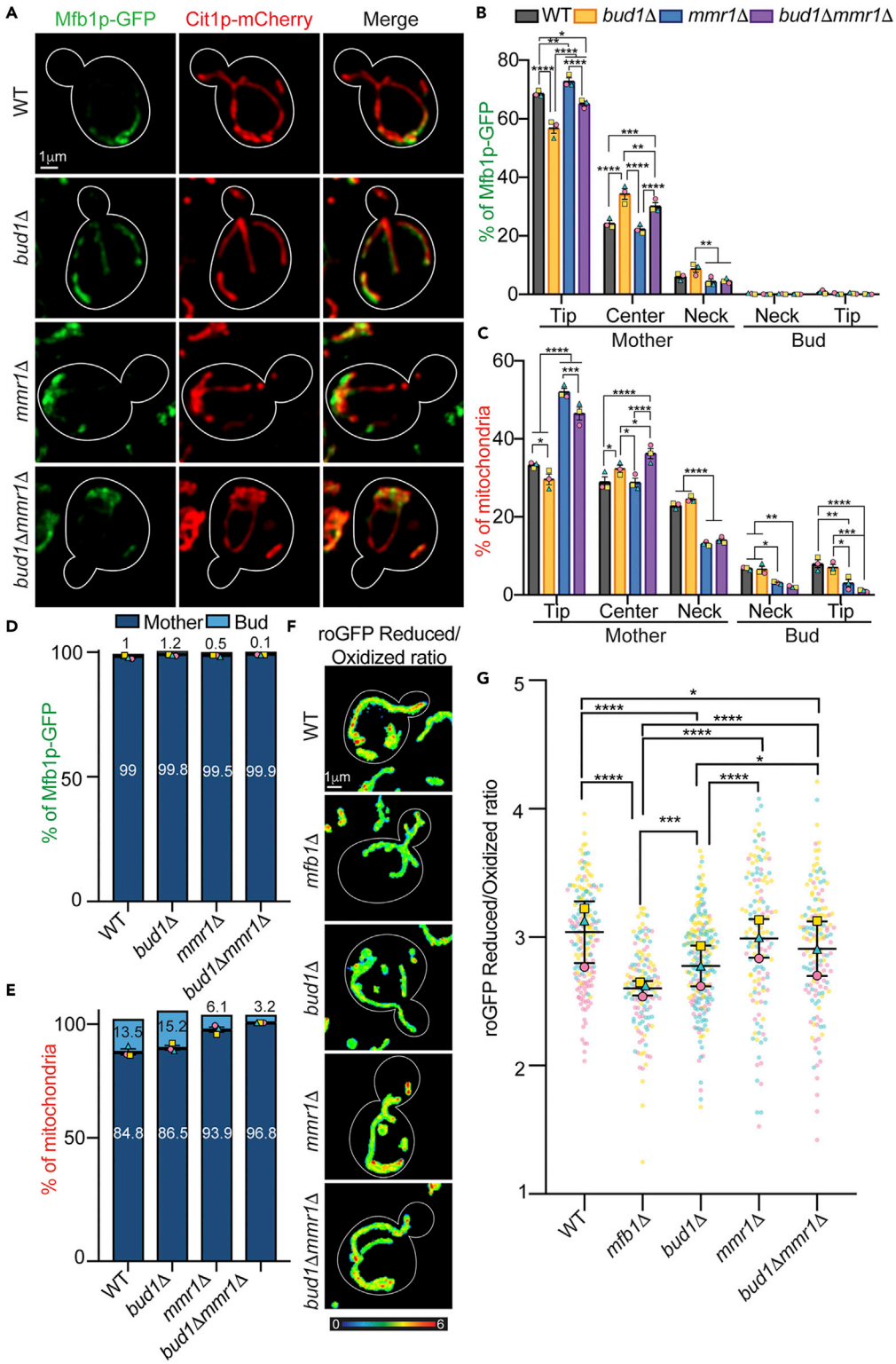

Figure 4. Deletion of *MMR1* rescues depolarized localization of Mfb1p, defects in mitochondrial distribution, and decreased mitochondrial quality in *bud1*Δ cells

(A) Representative images of Mfb1p (green) and mitochondria (red) in mid-log phase WT, *bud1*Δ, *mmr1*Δ, or *bud1*Δ *mmr1*Δ cells visualized as for Figure 2A. Cell outlines: white. Scale bars: 1 μm.

Figure 4. *Continued*

(B–E) ROIs are defined as for Figure 2B. n >50 cells/strain/trial. The mean ± SEM of three independent trials is shown with differently shaped and colored symbols for each trial. p <0.0001 (one-way ANOVA with Tukey's multiple comparisons test). p values are denoted as: ****p <0.0001; ***p <0.001; **p <0.01; *p <0.05. (B, C, D, and E) Relative distribution of Mfb1p-GFP and mitochondria in WT, *bud1*Δ, *mmr1*Δ, or *bud1*Δ *mmr1*Δ cells at specific regions within the cell (B and C) or in mother cells and buds (D and E).

(F) Maximum projections of ratiometric images of reduced/oxidized integrated mito-roGFP1 in mid-log phase WT, *mfb1*Δ, *bud1*Δ, *mmr1*Δ, or *bud1*Δ *mmr1*Δ cells. Colors reflect the intensity of the ratio of reduced-to-oxidized mito-roGFP1 (scale at the bottom). Cell outlines: white. n >50 cells/strain/trial.

(G) Quantification of reduced/oxidized mito-roGFP1 of mitochondria in mother cells of genotypes or treatments shown in (F). The means of three independent trials are shown, with differently shaped and colored symbols for each trial. Mean ± SEM of the ratio of reduced/oxidized mito-roGFP1: 3.042 ± 0.1388 (WT), 2.605 ± 0.0333 (*mfb1*Δ), 2.779 ± 0.0912 (*bud1*Δ), 2.992 ± 0.0868 (*mmr1*Δ), 2.914 ± 0.1227 (*bud1*Δ *mmr1*Δ). p <0.0438 (one-way ANOVA with Tukey's multiple comparisons test). p values are denoted as: ****p <0.0001; ***p <0.001; **p <0.01; *p <0.05.

function in anchorage of mitochondria in the mother cell tip, but not its binding to mitochondria or asymmetric distribution between buds and mother cells, is dependent on Bud1p/Rsr1p. Equally important, the mitochondrial phenotypes associated with deletion of *BUD1* resemble those observed during early stages of yeast cell replicative aging.

To further explore the relationship of the bud site selection machinery to Mfb1p and its function in mitochondrial distribution, we studied the effect of deletion of *BUD2* and *BUD5*, genes that regulate Bud1p, in these processes. As expected, deletion of *BUD2* or *BUD5* results in random bud site selection (Figure S5A). Moreover, we found that the phenotypes observed in *bud2*Δ and *bud5*Δ cells are similar to those observed in *bud1*Δ cells and during early stages of aging. Deletion of *BUD2* or *BUD5* results in defects in polarization of Mfb1p and mitochondria within mother cells (Figures S5B, S5E, and S5F) but has no effect on the asymmetric distribution of Mfb1p or mitochondria between mother cells and buds (Figures S5C and S5D).

Next, we tested whether loss of bud site selection affects mitochondrial function, using mitochondria-targeted redox-sensing GFP (mito-roGFP1) (Figures 3D and 3E). We confirmed that deletion of *MFB1* results in reduced mitochondrial redox state: the ratio of reduced to oxidized mito-roGFP1 in *mfb1*Δ cells is 20% lower than that observed in WT cells. Beyond this, we found that mitochondrial redox state in *bud1*Δ, *bud2*Δ, and *bud5*Δ cells is decreased compared to WT mother cells but greater than that observed in *mfb1*Δ cells (Figures 3D, 3E, S5G, and S5H). Finally, in *bud1*Δ cells, mitochondria at the mother cell tip are not significantly higher-functioning compared to other mitochondria within the mother cell (Figure S6). Thus, mutation of bud site selection genes compromises the function of mitochondria not just in the mother cell tip but throughout the yeast mother cell.

Deletion of *MMR1* rescues defects in Mfb1p and mitochondrial distribution as well as mitochondrial quality control observed in *bud1*Δ mutants

The premature aging phenotype of *mfb1*Δ has been attributed to the disproportionate loss of higher-functioning mitochondria from mother cells (Pernice et al., 2016). Deleting the cargo adaptor and bud tip mitochondrial tether, *MMR1*, can effectively reduce the amount of mitochondria transferred to and retained in buds, and thus rescue the overall distribution of mitochondria between mother and bud as well as the mitochondrial quality defects observed upon deletion of *MFB1* (Chernyakov et al., 2013; Itoh et al., 2004; Pernice et al., 2016; Swayne et al., 2011). Therefore, if the reduced fitness and lifespan observed in *bud1*Δ cells are a consequence of depolarization of Mfb1p within mother cells and the associated defects in retention of higher-functioning mitochondria in the mother cell, then deletion of *MMR1* should rescue the defects in mitochondrial distribution and quality observed in a bud site selection mutant.

To examine this possibility, we deleted the *MMR1* gene in *bud1*Δ and compared the phenotypes observed in *bud1*Δ *mmr1*Δ cells to those in *bud1*Δ or *mmr1*Δ single mutants and to WT cells. Deletion of *MMR1* does not change the overall distribution of Mfb1p between mother and bud cells (Figures 4A and 4D). However, it increases the abundance of mitochondria in mother cells (Figures 4A and 4E) and in the distal tip area of mother cells (Figures 4A and 4C). Intriguingly, analysis of the *bud1*Δ *mmr1*Δ mutant revealed that deletion of *MMR1* partially restores the defects in accumulation of mitochondria and Mfb1p at the mother distal tip of *bud1*Δ cells (Figures 4A and 4B). Finally, deletion of *MMR1* rescues the defect in mitochondrial quality in

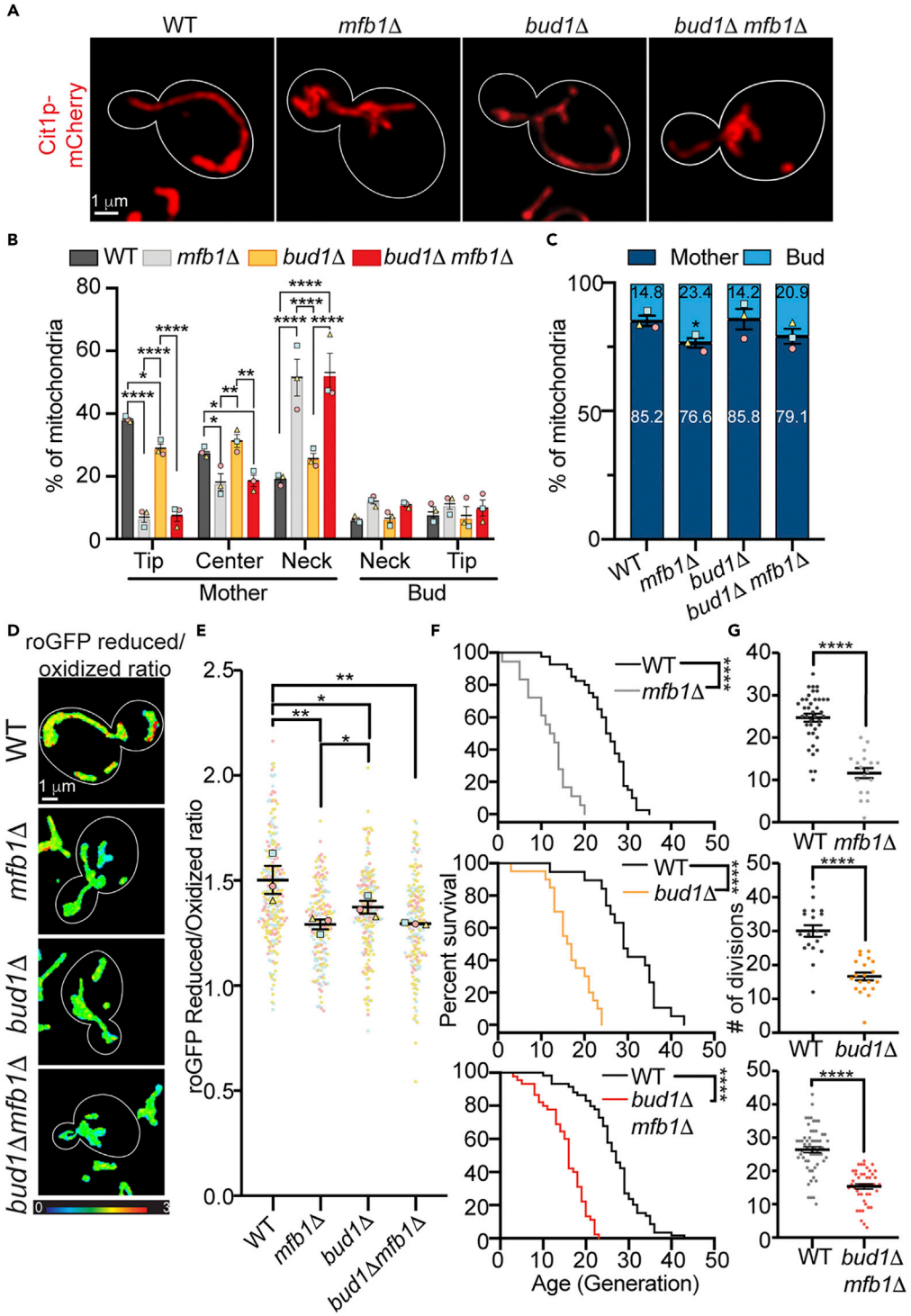

Figure 5. *BUD1* and *MFB1* function in the same pathway for mitochondrial distribution and quality control and RLS

(A) Maximum projections of mitochondria visualized using Cit1p-mCherry in mid-log phase WT, *mfb1*Δ, *bud1*Δ, and *bud1*Δ *mfb1*Δ cells. Cell outlines: white. Scale bars: 1 μm.

(B and C) Quantification of the mitochondrial distribution of (A). ROIs are defined in Figure 2C. >21 cells/strain/trial. Data are represented as mean ± SEM The means of three independent trials are shown in different shaped and colored

Figure 5. *Continued*

symbols for each trial. p < 0.0001 (one-way ANOVA with Tukey's multiple comparisons test). p values are denoted as: ****p <0.0001; ***p <0.001; **p <0.01; *p <0.05.

(D) Maximum projections of ratiometric images of reduced/oxidized integrated mito-roGFP1 in mid-log phase WT, *mfb1*Δ, *bud1*Δ, and *bud1*Δ *mfb1*Δ cells. Colors reflect the intensity of the ratio of reduced-to-oxidized mito-roGFP1 (scale at the bottom right). Cell outlines: white. n >48 cells/strain/trial.

(E) Quantification of reduced/oxidized mito-roGFP1 of mitochondria in mother cells of indicated genotypes from panel (D). The mean of three independent trials with differently shaped and colored symbols for each trial. Mean ± SEM of the ratio of reduced/oxidized mito-roGFP1: 1.505 ± 0.0669 (WT), 1.293 ± 0.0235 (*mfb1*Δ), 1.375 ± 0.0297 (*bud1*Δ), 1.296 ± 0.297 (*bud1*Δ *mfb1*Δ). p <0.0004 (one-way ANOVA with Tukey's multiple comparisons test). p values are denoted as: ****p <0.0001; ***p <0.001; **p <0.01; *p <0.05.

(F) Kaplan-Meier survival plots of replicative lifespans (RLS) of WT (black line), *mfb1*Δ (gray line), *bud1*Δ (orange line), and *bud1*Δ *mfb1*Δ (red line) were generated by counting the number of daughter cells produced from virgin mother cells. Data shown here is one representative trial. n >20 cells/strain/experiment for two independent trials. p value <0.0001 (Mantel-Cox test).

(G) Scatterplot displaying the total number of divisions generated by the mother cells in each genotype in (F).

mother cells and buds produced by deletion of *BUD1* (Figures 4F and 4G). Taken together, we find that inhibition of mitochondrial inheritance by deletion of *MMR1* rescues the overall defects in mitochondrial distribution and function produced by loss of *BUD1*.

BUD1 and *MFB1* act in the same pathway to regulate mitochondria and lifespan

Because mitochondria are aging determinants, it is possible that the bud site selection machinery contributes to lifespan control through effects on Mfb1p function in mitochondrial distribution and quality control. Indeed, we find that deletion of *BUD1* or *MFB1* results in similar phenotypes: defects in accumulation of mitochondria in the mother cell tip without affecting overall asymmetric distribution of the organelle between mother cells and buds, and defects in mitochondrial function throughout the yeast cell. We also find that bud site selection and Mfb1p polarization within mother cells both decline with age and observe striking similarities in those declines. Specifically, both processes decline at similar stages early in the yeast aging process and reach a plateau later in aging.

Here, we used analysis of epistatic interactions to determine whether the bud site selection machinery and Mfb1p function in the same pathway for control of mitochondrial distribution and quality control. If this hypothesis is correct, then defects in accumulation of mitochondria in the mother cell tip and mitochondrial redox state observed in the *bud1*Δ *mfb1*Δ double mutant should not be greater than defects observed in either single mutant. Indeed, we obtained evidence for epistasis between *BUD1* and *MFB1* (Figures 5A–5E). Specifically, we found that the distribution of mitochondria, accumulation of the organelle in the mother cell tip and the redox state of mitochondria in the mother cell and bud are similar in *bud1*Δ *mfb1*Δ and *mfb1*Δ cells. Here too, we find that the phenotype observed in *bud1*Δ cells is less severe than that observed in *mfb1*Δ cells: mitochondrial distribution and redox state are both compromised in *bud1*Δ cells, but to a lesser extent than that observed in *mfb1*Δ cells. Moreover, we found that mitochondrial defects observed in *bud1*Δ *mfb1*Δ and *mfb1*Δ cells are greater than those observed in *bud1*Δ cells. However, the double *bud1*Δ *mfb1*Δ mutant is not significantly different from the *mfb1*Δ single mutant.

Finally, we used epistasis analysis to determine whether *BUD1* and *MFB1* function in the same pathway for RLS control (Figures 5F and 5G). If deletion of *BUD1* affects lifespan through effects on Mfb1p function, then deletion of both genes will not have additive effects on RLS compared to single mutants. We find that the mean RLS of WT, *bud1*Δ and *mfb1*Δ single mutants, and *bud1*Δ *mfb1*Δ double mutants are 26.7 ± 7.51, 17.15 ± 4.94, 12.1 ± 5.01, and 15.33 ± 5.10 generations, respectively. Thus, we confirmed that deletion of *BUD1* or *MFB1* results in a significant decrease in yeast RLS. In addition, we find that RLS of the *bud1*Δ *mfb1*Δ double mutant is similar to that observed in the *mfb1*Δ single mutant and that the reduction in RLS observed in the *bud1*Δ *mfb1*Δ double mutant is not more severe than that observed in either *bud1*Δ or *mfb1*Δ single mutants. These findings provide genetic evidence that *MFB1* and *BUD1* function in the same pathway for control of mitochondrial distribution and quality control and for RLS in yeast.

DISCUSSION

Cell polarity during asymmetric cell division declines with age. For example, stem cell division becomes more symmetric in aged mice, indicating a more depolarized phenotype (Florian et al., 2018). Cell division

also becomes more symmetric with replicative age in yeast, which leads to premature aging in daughter cells (Kennedy et al., 1994). Moreover, specific components of the cell polarity machinery change with age. Cdc42 activity increases with age in hematopoietic stem cells, and inhibition of Cdc42 reduces aging phenotypes observed in those cells (Florian et al., 2012). Similarly, actin cables, the tracks for cargo movement during polarized cell division in yeast, undergo age-linked declines in stability and polarity (Sing et al., 2021).

The bud site selection machinery drives breaking of cell symmetry at the onset of polarity establishment during asymmetric cell division in yeast. Analysis of the mechanism underlying bud site selection has revealed different patterns for symmetry breaking in haploid and diploid yeast, the landmarks for bud site selection, the proteins that mediate those processes, and how bud site selection activates reorganization of the cytoskeleton to the selected polarity site. Moreover, studies in multicellular organisms indicate that symmetry breaking and defining polarity planes are critical for establishing directional dues for development. However, the benefit of bud site selection for yeast, a single-celled organism, is not well understood.

Here, we provide evidence that bud site selection fidelity declines with age. Moreover, we identified a known aging determinant, mitochondria, as a target for the bud site selection machinery. We found that disabling axial bud site selection alters the polarized localization of Mfb1p within mother cells but has no effect on asymmetric distribution of Mfb1p between mother cells and buds. We also found that loss of bud site selection results in defects in Mfb1p function in mitochondrial distribution and quality, and in yeast lifespan control. Finally, we obtained evidence that there is a distinctive posterior pole in asymmetrically dividing haploid yeast and that the distal tip of the mother cell is that pole.

Age-associated declines in polarity site selection in yeast

Early evidence indicates that polarized bud site selection may decline with age (Jazwinski et al., 1998). However, resolution of bud site selection was limited in early studies. We revisited this topic using approaches for more effective, noninvasive isolation of yeast of different replicative ages, and for visualization of individual bud site selection events during the aging process with greater temporal resolution. Our studies provide definitive evidence that polarized bud site selection declines with age in yeast.

Our study also demonstrates that the decline in budding polarity in aging yeast is not linear. The bud site selection machinery is robust in younger cells (1-5 generations). This is expected because stringent bud site selection is evident in mid-log phase yeast, which are primarily young cells. However, we detect a significant increase in random bud site selection early in the aging process (>5 generations). The age-associated decline in bud site selection does not appear to be because of changes in *BUD1* gene expression: two independent studies on changes in the yeast transcriptome and proteome with age indicate that *BUD1* mRNA and protein levels remain constant during the yeast RLS (Hendrickson et al., 2018; Janssens et al., 2015). On the other hand, studies from our lab and others indicate that age-linked declines in established aging determinants are evident early in the yeast RLS and may therefore cause or be major contributors to the aging process (Henderson et al., 2014; Hughes and Gottschling, 2012; McFaline-Figueroa et al., 2011). Here, we find that the decline in bud site selection fidelity occurs early in replicative aging and in the same time frame as age-linked changes in other aging determinants. These findings are consistent with a causative role for declines in bud site selection in yeast cell aging.

Interestingly, this decline in axial bud site selection reaches a plateau at 10–20 generations and does not decline further as cells age. Previous studies indicate that a cell that undergoes random budding events can exhibit polarized bud site selection at subsequent rounds of cell division (Jazwinski et al., 1998). This finding raises the possibility that the polarity of bud site selection is not lost irrevocably with age. Rather, the stringency of this process may decline with age. The plateau in polarized bud site selection observed in yeast at advanced age may be a consequence of the reduced stringency of this aspect of polarity establishment in yeast.

Age-associated declines in Mfb1p localization and function in control of mitochondria

Our previous studies revealed that Mfb1p functions as a tether that anchors a small population of higher-functioning mitochondria in the mother cell tip, and that this process is required to retain some higher-functioning mitochondria in mother cells, which in turn is required for mother cell fitness and lifespan (Pernice et al., 2016). Our previous studies also revealed an age-linked decline in mitochondrial function in

yeast (McFaline-Figueroa et al., 2011) and that defects in mitochondrial quality control can result in premature aging in yeast (Higuchi et al., 2013). Here, we find that Mfb1p function in binding to mitochondria does not decline with age. However, we detect an age-associated decline in Mfb1p's function as a region-specific mitochondrial tether: accumulation of Mfb1p and mitochondria in the mother cell tip diminishes with age. The age-associated declines in Mfb1p localization and function in the mother cell tip do not appear to be because of changes in *MFB1* gene expression: analysis of changes in the yeast transcriptome with age indicate that *MFB1* mRNA levels remain constant during the yeast replicative lifespan (Hendrickson et al., 2018; Janssens et al., 2015).

Moreover, we find that the decline in Mfb1p localization at the mother cell tip occurs early in the aging process, at the same stage as age-linked declines in bud site selection. Indeed, we find that defects in Mfb1p localization also reach a plateau, similar to the plateau observed in age-linked declines in bud site selection. These findings reveal temporal links between aging of the bud site selection machinery and Mfb1p. Moreover, because declines in bud site selection and Mfb1p localization and function occur early in RLS, it is possible that these changes contribute to the aging process.

Finally, inheritance of higher-functioning mitochondria by yeast daughter cells persists during the aging process (McFaline-Figueroa et al., 2011) and is not compromised by deletion of *MFB1* or *BUD1*. Moreover, asymmetric inheritance of Mfb1p between mother cells and buds is not affected by loss of the bud site selection machinery and does not decline with age. Therefore, Mfb1p and bud site selection function in lifespan control is not because of effects on asymmetric inheritance of mitochondria or Mfb1p. Rather, they are because of defects in polarization of Mfb1p and mitochondria within the mother cell, and the consequences of these defects on mitochondrial function.

Overall, there are multiple mechanisms to ensure that higher functioning mitochondria are inherited by yeast daughter cells. Higher functioning mitochondria exhibit higher motility activity and are preferentially transferred from mother to daughter cell (Higuchi et al., 2013). In addition, newly inherited higher functioning mitochondria are retained in daughter cells by anchorage in the bud tip (Swayne et al., 2011). Finally, any lower functioning, less motile mitochondria that enter daughter cells are transported from buds to mother cells (Higuchi et al., 2013). However, there is only one known mechanism to ensure that healthy mitochondria are retained in mother cells: Mfb1-mediated anchorage of higher functioning mitochondria in the mother cell tip. This process affects the fitness and lifespan of mother cells. Moreover, although daughter cells preferentially inherit the fittest mitochondria from mother cells and this process persists in *mfb1*Δ and *bud1*Δ cells, a decline in mitochondrial function in mother cells impacts on all progeny produced from mother cells.

Role for the bud site selection machinery in mitochondrial quality control and lifespan

Our findings also support a role for polarized bud site selection in yeast lifespan control through effects on Mfb1p-dependent mitochondrial quality control. Specifically, we find that deletion of *BUD1*, *BUD2*, or *BUD5* results in defects in localization of Mfb1p to the mother distal tip, defects in anchorage of mitochondria at that site and a decrease in mitochondrial function throughout yeast cells. Moreover, we found that deletion of *MMR1*, a protein implicated in movement of mitochondria from mother cells to buds and anchorage-dependent retention of newly inherited mitochondria the bud tip (Chernyakov et al., 2013; Itoh et al., 2004; Swayne et al., 2011), restores the defects in mitochondrial distribution and overall quality observed upon deletion of *BUD1*. Thus, our findings support a role for the bud site selection machinery in mitochondria quality control through effects on mitochondrial distribution.

Although there are clear links between the bud site selection machinery and Mfb1p functions in mitochondrial distribution and quality control, loss of bud site selection activity produces significantly less severe defects on mitochondrial distribution and function compared to deletion of *MFB1*. However, as described above, loss of bud site selection does not inhibit establishment of cell polarity or polarized cell division in yeast. Consistent with this, asymmetric distribution of Mfb1p between mother cells and buds is not compromised in *bud1*Δ, *bud2*Δ, or *bud5*Δ mutants. Moreover, deletion of bud site selection proteins does not affect association of Mfb1p with mitochondria. Thus, Mfb1p is present, active, and asymmetrically distributed in cells with no bud site selection machinery. Therefore, it is possible that the defects observed in *bud1*Δ, *bud2*Δ, or *bud5*Δ cells are less severe that those observed in *mfb1*Δ because Mfb1p can still promote some anchorage and retention of mitochondria in mother cells in the absence of bud site selection cues.

We also obtained genetic evidence that *BUD1* and *MFB1* function in the same pathway for mitochondrial distribution and quality control and on lifespan. First, we observed that aging has similar effects on bud site selection and Mfb1p polarization within mother cells. In both cases, declines are evident early in the aging process and reach a plateau in cells of advanced age. Second, deletion of either *BUD1* or *MFB1* produces similar effects on mitochondrial distribution, anchorage of mitochondria in the mother cell tip, mitochondrial redox state, and RLS. Moreover, deletion of both genes has no additive effect on those phenotypes compared to *mfb1*Δ or *bud1*Δ single mutants. Finally, we found that deletion of *MMR1* and the associated decrease in mitochondrial inheritance by daughter cells rescues the polarized mitochondrial and Mfb1p distribution and defects in mitochondrial function observed in *bud1*Δ cells. This supports a critical role for bud site selection in mitochondrial quality control during inheritance. Thus, we conclude that the reduced lifespan produced by loss of polarized bud site selection is because of effects on Mfb1p function in mitochondrial quality control.

Is the mother distal tip the posterior pole during asymmetric cell division in haploid yeast?

During the establishment of cell polarity in model systems including frog and worm embryos, the cytoskeleton is reorganized leading to polarized localization of cortical proteins at anterior and posterior poles of the cell. Diploid yeast exhibit bipolar budding patterns (i.e., bud site selection either adjacent to or at opposite poles from the previous bud site) and asymmetric distribution of polarity factors at anterior and posterior poles of the cell (Chant and Pringle, 1991; Chiou et al., 2017; Kang et al., 2004). However, haploid yeast undergoes axial or unipolar bud site selection: each new bud is produced adjacent to the previous bud site. The bud tip is an established anterior pole and site for activation of polarity factors including Cdc42p and its effectors in haploid and diploid yeast. However, there is no obvious localization of polarity factors to a posterior pole in a haploid yeast cell. We find that the bud site selection machinery is required for 1) targeting of Mfb1p to the mother cell tip, 2) Mfb1p function in anchorage of higher-functioning mitochondria at the mother cell tip, and 3) RLS control through effects on Mfb1p localization and function. These observations support the model that a posterior pole exists in haploid yeast cells and that the mother cell tip is that pole.

Limitations of the study

Bud sites are selected by related but distinct mechanisms in haploid and diploid yeast cells: haploid cells exhibit axial budding whereas diploid cells exhibit bipolar budding. These studies were carried out in haploid yeast cells. In addition, these studies were carried out in the S288c genetic background. Previous studies indicate that the W303 yeast strain, which carries a mutation in the bud site selection gene *BUD4* (Voth et al., 2005), exhibits defects in asymmetric distribution of Mfb1p (Kondo-Okamoto et al., 2006, 2007).

STAR★METHODS

Detailed methods are provided in the online version of this paper and include the following:

- KEY RESOURCES TABLE
- RESOURCE AVAILABILITY
  - Lead contact
  - Material availability
  - Data and code availability
- EXPERIMENTAL MODEL AND SUBJECT DETAILS
  - Yeast growth conditions
  - Yeast strain construction
- METHOD DETAILS
  - Microscopy
  - Visualization of bud scars
  - Enrichment of aged cells
  - Enrichment of aged cells in the miniature-chemostat aging device and assessment of bud site selection
  - Analysis of mitochondrial and Mfb1p distribution
  - Analysis of co-localization of Mfb1p and mitochondria
  - Analysis of mitochondrial redox state
  - Analysis of replicative lifespan
- QUANTIFICATION AND STATISTICAL ANALYSIS

SUPPLEMENTAL INFORMATION

Supplemental information can be found online at https://doi.org/10.1016/j.isci.2022.103957.

ACKNOWLEDGMENTS

We thank members of the Pon laboratory for technical assistance and valuable discussion. This work was supported by awards from the National Institutes of Health (NIH) (GM45735, GM122589, and AG051047) to L.A.P. We also thank Dr. Theresa Swayne in the Confocal and Specialized Microscopy Shared Resource for valuable discussion. The Confocal and Specialized Microscopy Shared Resource in the Herbert Irving Comprehensive Cancer Center at Columbia University is supported in part by an award from the NIH/NCI (P30 CA13696).

AUTHOR CONTRIBUTIONS

Conceptualization, E.J.Y., W.M.P., and L.A.P.; Formal Analysis, E.J.Y. and W.M.P.; Investigation, E.J.Y. and W.M.P.; Writing – Original Draft, E.J.Y.; Writing – Review & Editing, E.J.Y., W.M.P., and L.A.P.; Funding Acquisition, L.A.P.; Supervision, L.A.P.

DECLARATION OF INTERESTS

The authors declare no competing interests.

Received: May 24, 2021
Revised: December 15, 2021
Accepted: February 17, 2022
Published: March 18, 2022

REFERENCES

Alvaro, D., Lisby, M., and Rothstein, R. (2007). Genome-wide analysis of Rad52 foci reveals diverse mechanisms impacting recombination. PLoS Genet. *3*, e228. https://doi.org/10.1371/journal.pgen.0030228.

Bähler, J., Wu, J.Q., Longtine, M.S., Shah, N.G., McKenzie, A., Steever, A.B., Wach, A., Philippsen, P., and Pringle, J.R. (1998). Heterologous modules for efficient and versatile PCR-based gene targeting in Schizosaccharomyces pombe. Yeast *14*, 943–951. https://doi.org/10.1002/(SICI)1097-0061(199807)14:10<943::AID-YEA292>3.0.CO;2-Y.

Bender, A. (1993). Genetic evidence for the roles of the bud-site-selection genes BUD5 and BUD2 in control of the Rsr1p (Bud1p) GTPase in yeast. Proc. Natl. Acad. Sci. U S A *90*, 9926–9929. https://doi.org/10.1073/pnas.90.21.9926.

Bender, A., and Pringle, J.R. (1989). Multicopy suppression of the cdc24 budding defect in yeast by CDC42 and three newly identified genes including the ras-related gene RSR1. Proc. Natl. Acad. Sci. U S A *86*, 9976–9980. https://doi.org/10.1073/pnas.86.24.9976.

Bi, E., and Park, H.-O. (2012). Cell polarization and cytokinesis in budding yeast. Genetics *191*, 347–387. https://doi.org/10.1534/genetics.111.132886.

Campos, S.E., Avelar-Rivas, J.A., Garay, E., Juárez-Reyes, A., and DeLuna, A. (2018). Genomewide mechanisms of chronological longevity by dietary restriction in budding yeast. Aging Cell *17*, e12749. https://doi.org/10.1111/acel.12749.

Chant, J., Corrado, K., Pringle, J.R., and Herskowitz, I. (1991). Yeast BUD5, encoding a putative GDP-GTP exchange factor, is necessary for bud site selection and interacts with bud formation gene BEM1. Cell *65*, 1213–1224. https://doi.org/10.1016/0092-8674(91)90016-r.

Chant, J., and Herskowitz, I. (1991). Genetic control of bud site selection in yeast by a set of gene products that constitute a morphogenetic pathway. Cell *65*, 1203–1212. https://doi.org/10.1016/0092-8674(91)90015-q.

Chant, J., and Pringle, J.R. (1995). Patterns of bud-site selection in the yeast Saccharomyces cerevisiae. J. Cell Biol. *129*, 751–765. https://doi.org/10.1083/jcb.129.3.751.

Chant, J., and Pringle, J.R. (1991). Budding and cell polarity in Saccharomyces cerevisiae. Curr. Opin. Genet. Dev. *1*, 342–350. https://doi.org/10.1016/s0959-437x(05)80298-9.

Chernyakov, I., Santiago-Tirado, F., and Bretscher, A. (2013). Active segregation of yeast mitochondria by Myo2 is essential and mediated by Mmr1 and Ypt11. Curr. Biol. *23*, 1818–1824. https://doi.org/10.1016/j.cub.2013.07.053.

Chiou, J.-G., Balasubramanian, M.K., and Lew, D.J. (2017). Cell polarity in yeast. Annu. Rev. Cell Dev. Biol. *33*, 77–101. https://doi.org/10.1146/annurev-cellbio-100616-060856.

Clay, L., Caudron, F., Denoth Lippuner, A., Boettcher, B., Buvelot Frei, S., Snapp, E.L., and Barral, Y. (2014). A sphingolipid-dependent diffusion barrier confines ER stress to the yeast mother cell. Elife *3*, e01883. https://doi.org/10.7554/eLife.01883.

Dürr, M., Escobar-Henriques, M., Merz, S., Geimer, S., Langer, T., and Westermann, B. (2006). Nonredundant roles of mitochondria-associated F-box proteins Mfb1 and Mdm30 in maintenance of mitochondrial morphology in yeast. Mol. Biol. Cell *17*, 3745–3755. https://doi.org/10.1091/mbc.e06-01-0053.

Erjavec, N., Cvijovic, M., Klipp, E., and Nyström, T. (2008). Selective benefits of damage partitioning in unicellular systems and its effects on aging. Proc. Natl. Acad. Sci. U S A *105*, 18764–18769. https://doi.org/10.1073/pnas.0804550105.

Fehrenbacher, K.L., Yang, H.-C., Gay, A.C., Huckaba, T.M., and Pon, L.A. (2004). Live cell imaging of mitochondrial movement along actin cables in budding yeast. Curr. Biol. *14*, 1996–2004. https://doi.org/10.1016/j.cub.2004.11.004.

Florian, M.C., Dörr, K., Niebel, A., Daria, D., Schrezenmeier, H., Rojewski, M., Filippi, M.-D., Hasenberg, A., Gunzer, M., Scharffetter-Kochanek, K., et al. (2012). Cdc42 activity regulates hematopoietic stem cell aging and rejuvenation. Cell Stem Cell *10*, 520–530. https://doi.org/10.1016/j.stem.2012.04.007.

Florian, M.C., Klose, M., Sacma, M., Jablanovic, J., Knudson, L., Nattamai, K.J., Marka, G., Vollmer, A., Soller, K., Sakk, V., et al. (2018). Aging alters the epigenetic asymmetry of HSC division. PLoS Biol. *16*, e2003389. https://doi.org/10.1371/journal.pbio.2003389.

Gardner, J.M., and Jaspersen, S.L. (2014). Manipulating the yeast genome: deletion, mutation, and tagging by PCR. In Ubiquitin Family Modifiers and the Proteasome, Methods in Molecular Biology (Springer New York),

pp. 45–78. https://doi.org/10.1007/978-1-4939-1363-3_5.

Gauss, R., Trautwein, M., Sommer, T., and Spang, A. (2005). New modules for the repeated internal and N-terminal epitope tagging of genes in Saccharomyces cerevisiae. Yeast *22*, 1–12. https://doi.org/10.1002/yea.1187.

Gietz, R.D., and Woods, R.A. (2002). Transformation of yeast by lithium acetate/single-stranded carrier DNA/polyethylene glycol method. Meth. Enzymol. *350*, 87–96. https://doi.org/10.1016/s0076-6879(02)50957-5.

Gueldener, U., Heinisch, J., Koehler, G.J., Voss, D., and Hegemann, J.H. (2002). A second set of loxP marker cassettes for Cre-mediated multiple gene knockouts in budding yeast. Nucleic Acids Res. *30*. e23-23. https://doi.org/10.1093/nar/30.6.e23.

Henderson, K.A., Hughes, A.L., and Gottschling, D.E. (2014). Mother-daughter asymmetry of pH underlies aging and rejuvenation in yeast. Elife *3*, e03504. https://doi.org/10.7554/eLife.03504.

Hendrickson, D.G., Soifer, I., Wranik, B.J., Kim, G., Robles, M., Gibney, P.A., and McIsaac, R.S. (2018). A new experimental platform facilitates assessment of the transcriptional and chromatin landscapes of aging yeast. Elife *7*. pdb.prot4169. https://doi.org/10.7554/eLife.39911.

Higuchi, R., Vevea, J.D., Swayne, T.C., Chojnowski, R., Hill, V., Boldogh, I.R., and Pon, L.A. (2013). Actin dynamics affect mitochondrial quality control and aging in budding yeast. Curr. Biol. *23*, 2417–2422. https://doi.org/10.1016/j.cub.2013.10.022.

Hughes, A.L., and Gottschling, D.E. (2012). An early age increase in vacuolar pH limits mitochondrial function and lifespan in yeast. Nature *492*, 261–265. https://doi.org/10.1038/nature11654.

Itoh, T., Toh-E, A., and Matsui, Y. (2004). Mmr1p is a mitochondrial factor for Myo2p-dependent inheritance of mitochondria in the budding yeast. EMBO J. *23*, 2520–2530. https://doi.org/10.1038/sj.emboj.7600271.

Janssens, G.E., Meinema, A.C., González, J., Wolters, J.C., Schmidt, A., Guryev, V., Bischoff, R., Wit, E.C., Veenhoff, L.M., and Heinemann, M. (2015). Protein biogenesis machinery is a driver of replicative aging in yeast. Elife *4*, e08527. https://doi.org/10.7554/eLife.08527.

Jazwinski, S.M., Kim, S., Lai, C.Y., and Benguria, A. (1998). Epigenetic stratification: the role of individual change in the biological aging process. Exp. Gerontol. *33*, 571–580. https://doi.org/10.1016/s0531-5565(98)00029-1.

Kang, P.J., Angerman, E., Nakashima, K., Pringle, J.R., and Park, H.-O. (2004). Interactions among Rax1p, Rax2p, Bud8p, and Bud9p in marking cortical sites for bipolar bud-site selection in yeast. Mol. Biol. Cell *15*, 5145–5157. https://doi.org/10.1091/mbc.e04-07-0600.

Kang, P.J., Sanson, A., Lee, B., and Park, H.O. (2001). A GDP/GTP exchange factor involved in linking a spatial landmark to cell polarity. Science *292*, 1376–1378. https://doi.org/10.1126/science.1060360.

Katajisto, P., Döhla, J., Chaffer, C.L., Pentinmikko, N., Marjanovic, N., Iqbal, S., Zoncu, R., Chen, W., Weinberg, R.A., and Sabatini, D.M. (2015). Asymmetric apportioning of aged mitochondria between daughter cells is required for stemness. Science *348*, 340–343. https://doi.org/10.1126/science.1260384.

Kennedy, B.K., Austriaco, N.R., and Guarente, L. (1994). Daughter cells of Saccharomyces cerevisiae from old mothers display a reduced life span. J. Cell Biol. *127*, 1985–1993. https://doi.org/10.1083/jcb.127.6.1985.

Kondo-Okamoto, N., Ohkuni, K., Kitagawa, K., McCaffery, J.M., Shaw, J.M., and Okamoto, K. (2006). The novel F-box protein Mfb1p regulates mitochondrial connectivity and exhibits asymmetric localization in yeast. Mol. Biol. Cell *17*, 3756–3767. https://doi.org/10.1091/mbc.e06-02-0145.

Kondo-Okamoto, N., Shaw, J.M., and Okamoto, K. (2007). Tetratricopeptide repeat proteins Tom70 and Tom71 mediate yeast mitochondrial morphogenesis. EMBO Rep. *9*, 63–69. https://doi.org/10.1038/sj.embor.7401113.

Kozubowski, L., Saito, K., Johnson, J.M., Howell, A.S., Zyla, T.R., and Lew, D.J. (2008). Symmetry-breaking polarization driven by a Cdc42p GEF-PAK complex. Curr. Biol. *18*, 1719–1726. https://doi.org/10.1016/j.cub.2008.09.060.

Liao, P.-C., Yang, E.J., and Pon, L.A. (2020). Live-cell imaging of mitochondrial redox state in yeast cells. STAR Protoc. *1*, 100160. https://doi.org/10.1016/j.xpro.2020.100160.

Lindstrom, D.L., and Gottschling, D.E. (2009). The mother enrichment program: a genetic system for facile replicative life span analysis in Saccharomyces cerevisiae. Genetics *183*, 413–422. 1SI–13SI. https://doi.org/10.1534/genetics.109.106229.

Longo, V.D., Shadel, G.S., Kaeberlein, M., and Kennedy, B. (2012). Replicative and chronological aging in Saccharomyces cerevisiae. Cell Metab. *16*, 18–31. https://doi.org/10.1016/j.cmet.2012.06.002.

Maxwell, C.S., and Magwene, P.M. (2017). The quick and the dead: microbial demography at the yeast thermal limit. Mol. Ecol. *26*, 1631–1640. https://doi.org/10.1111/mec.13955.

McFaline-Figueroa, J.R., Vevea, J., Swayne, T.C., Zhou, C., Liu, C., Leung, G., Boldogh, I.R., and Pon, L.A. (2011). Mitochondrial quality control during inheritance is associated with lifespan and mother-daughter age asymmetry in budding yeast. Aging Cell *10*, 885–895. https://doi.org/10.1111/j.1474-9726.2011.00731.x.

Moseley, J.B., and Goode, B.L. (2006). The yeast actin cytoskeleton: from cellular function to biochemical mechanism. Microbiol. Mol. Biol. Rev. *70*, 605–645. https://doi.org/10.1128/MMBR.00013-06.

Novarina, D., Mavrova, S.N., Janssens, G.E., Rempel, I.L., Veenhoff, L.M., and Chang, M. (2017). Increased genome instability is not accompanied by sensitivity to DNA damaging agents in aged yeast cells. DNA Repair (Amst) *54*, 1–7. https://doi.org/10.1016/j.dnarep.2017.03.005.

Park, H.O., Chant, J., and Herskowitz, I. (1993). BUD2 encodes a GTPase-activating protein for Bud1/Rsr1 necessary for proper bud-site selection in yeast. Nature *365*, 269–274. https://doi.org/10.1038/365269a0.

Park, H.O., Sanson, A., and Herskowitz, I. (1999). Localization of Bud2p, a GTPase-activating protein necessary for programming cell polarity in yeast to the presumptive bud site. Genes Dev. *13*, 1912–1917. https://doi.org/10.1101/gad.13.15.1912.

Pernice, W.M., Vevea, J.D., and Pon, L.A. (2016). A role for Mfb1p in region-specific anchorage of high-functioning mitochondria and lifespan in Saccharomyces cerevisiae. Nat. Commun. *7*, 10595. https://doi.org/10.1038/ncomms10595.

Powers, S., Gonzales, E., Christensen, T., Cubert, J., and Broek, D. (1991). Functional cloning of BUD5, a CDC25-related gene from S. cerevisiae that can suppress a dominant-negative RAS2 mutant. Cell *65*, 1225–1231. https://doi.org/10.1016/0092-8674(91)90017-s.

Rose, L., and Gönczy, P. (2014). Polarity establishment, asymmetric division and segregation of fate determinants in early C. elegans embryos. WormBook, 1–43. https://doi.org/10.1895/wormbook.1.30.2.

Schindelin, J., Arganda-Carreras, I., Frise, E., Kaynig, V., Longair, M., Pietzsch, T., Preibisch, S., Rueden, C., Saalfeld, S., Schmid, B., et al. (2012). Fiji: an open-source platform for biological-image analysis. Nat. Methods *9*, 676–682. https://doi.org/10.1038/nmeth.2019.

Shepard, K.A., Gerber, A.P., Jambhekar, A., Takizawa, P.A., Brown, P.O., Herschlag, D., DeRisi, J.L., and Vale, R.D. (2003). Widespread cytoplasmic mRNA transport in yeast: identification of 22 bud-localized transcripts using DNA microarray analysis. Proc. Natl. Acad. Sci. U S A *100*, 11429–11434. https://doi.org/10.1073/pnas.2033246100.

Sherman, F. (2002). Getting started with yeast. Meth. Enzymol. *350*, 3–41. https://doi.org/10.1016/S0076-6879(02)50954-X.

Sinclair, D.A., Mills, K., and Guarente, L. (1997). Accelerated aging and nucleolar fragmentation in yeast sgs1 mutants. Science *277*, 1313–1316. https://doi.org/10.1126/science.277.5330.1313.

Sing, C.N., Garcia, E.J., Lipkin, T.G., Huckaba, T.M., Tsang, C.A., Coughlin, A.C., Yang, E.J., Boldogh, I.R., Higuchi-Sanabria, R., and Pon, L.A. (2021). Identification of a novel modulator of the actin cytoskeleton, mitochondria, nutrient metabolism and lifespan in yeast. bioRxiv. https://doi.org/10.1101/2021.10.07.463535.

Slaughter, B.D., Smith, S.E., and Li, R. (2009). Symmetry breaking in the life cycle of the budding yeast. Cold Spring Harbor Perspect. Biol. *1*, a003384. https://doi.org/10.1101/cshperspect.a003384.

Slubowski, C.J., Funk, A.D., Roesner, J.M., Paulissen, S.M., and Huang, L.S. (2015). Plasmids for C-terminal tagging in Saccharomyces cerevisiae that contain improved GFP proteins. Yeast *32*, 379–387. https://doi.org/10.1002/yea.3065.

Smeal, T., Claus, J., Kennedy, B., Cole, F., and Guarente, L. (1996). Loss of transcriptional silencing causes sterility in old mother cells of S. cerevisiae. Cell *84*, 633–642. https://doi.org/10.1016/s0092-8674(00)81038-7.

Swayne, T.C., Zhou, C., Boldogh, I.R., Charalel, J.K., McFaline-Figueroa, J.R., Thoms, S., Yang, C., Leung, G., McInnes, J., Erdmann, R., and Pon, L.A. (2011). Role for cER and Mmr1p in anchorage of mitochondria at sites of polarized surface growth in budding yeast. Curr. Biol. *21*, 1994–1999. https://doi.org/10.1016/j.cub.2011.10.019.

Vevea, J.D., Wolken, D.M.A., Swayne, T.C., White, A.B., and Pon, L.A. (2013). Ratiometric biosensors that measure mitochondrial redox state and ATP in living yeast cells. J. Vis. Exp. e50633. https://doi.org/10.3791/50633.

Voth, W.P., Olsen, A.E., Sbia, M., Freedman, K.H., and Stillman, D.J. (2005). ACE2, CBK1, and BUD4 in budding and cell separation. Eukaryot. Cell *4*, 1018–1028. https://doi.org/10.1128/EC.4.6.1018-1028.2005.

Wu, C.-F., and Lew, D.J. (2013). Beyond symmetry-breaking: competition and negative feedback in GTPase regulation. Trends Cell Biol. *23*, 476–483. https://doi.org/10.1016/j.tcb.2013.05.003.

Wu, C.-F., Savage, N.S., and Lew, D.J. (2013). Interaction between bud-site selection and polarity-establishment machineries in budding yeast. Philos. Trans. R. Soc. Lond. B Biol. Sci. *368*, 20130006. https://doi.org/10.1098/rstb.2013.0006.

Yang, H.C., Palazzo, A., Swayne, T.C., and Pon, L.A. (1999). A retention mechanism for distribution of mitochondria during cell division in budding yeast. Curr. Biol. *9*, 1111–1114. https://doi.org/10.1016/s0960-9822(99)80480-1.

Young, C.L., Raden, D.L., Caplan, J.L., Czymmek, K.J., and Robinson, A.S. (2012). Cassette series designed for live-cell imaging of proteins and high-resolution techniques in yeast. Yeast *29*, 119–136. https://doi.org/10.1002/yea.2895.

Zheng, Y., Bender, A., and Cerione, R.A. (1995). Interactions among proteins involved in bud-site selection and bud-site assembly in Saccharomyces cerevisiae. J. Biol. Chem. *270*, 626–630. https://doi.org/10.1074/jbc.270.2.626.

STAR★METHODS

KEY RESOURCES TABLE

REAGENT or RESOURCE	SOURCE	IDENTIFIER
Chemicals, peptides, and recombinant proteins		
KAPA HiFi PCR kit	Roche Sequencing and Life Science, Kapa Biosystems, Wilmington, MA	KK1006
Hygromycin B	Sigma-Aldrich, St. Louis, MO	H3274
Geneticin	Sigma-Aldrich, St. Louis, MO	A1720
Calcofluor® White M2R staining	Milipore Sigma, Burlington, MA	#18909
Wheat Germ Agglutinin, Alexa Fluor™ 488 Conjugate	Thermo Fisher Scientific, Waltham, MA	#W11261
Wheat Germ Agglutinin, Alexa Fluor™ 594 Conjugate	Thermo Fisher Scientific, Waltham, MA	#W11262
Wheat Germ Agglutinin, Alexa Fluor™ 647 Conjugate	Thermo Fisher Scientific, Waltham, MA	#W32466
EZ Link Sulfo-NHS-LC-LC-Biotin	Thermo Fisher Scientific, Waltham, MA	#21338
Miltenyi µMACs Streptavidin MicroBeads	Miltenyi Biotec Inc., Auburn, CA	#130-048-101
Miltenyi LS Columns	Miltenyi Biotec Inc., Auburn, CA	#130-042-401
Miltenyi MultiStand	Miltenyi Biotec Inc., Auburn, CA	#130-042-303
Miniature chemostat aging device (mCAD)	(Hendrickson et al., 2018)	
Dynabeads MyOne Streptavidin C1 beads	Thermo Fisher Scientific, Waltham, MA	#65001
Experimental models: Organisms/strains		
Please refer to Table S1		
Oligonucleotides		
Please refer to Table S2		
Recombinant DNA		
pFA6a-link-GFPEnvy-SpHis5	(Slubowski et al., 2015) Linda Huang lab	Addgene plasmid #60782
pCY3090-02	(Young et al., 2012) Anne Robinson lab	Addgene plasmid #36231
pFA6a-GFP(S65T)-KanMX6	(Bähler et al., 1998) Jurg Bahler and John Pringle lab	Addgene plasmid #39292
HO-pGPD-mito-roGFP-KanMX6-HO	(Liao et al., 2020)	
pOM13	(Gauss et al., 2005), Euroscarf	Euroscarf plasmid #P30388
pOM12	(Gauss et al., 2005), Euroscarf	Euroscarf plasmid #P30387
pSH62	(Gueldener et al., 2002), Euroscarf	Euroscarf plasmid #P30120
Software and algorithms		
Volocity 6.3	Quorum Technologies	https://www.quorumtechnologies.com/volocity/volocity-downloads/legacy
FIJI	(Schindelin et al., 2012)	https://imagej.net/Fiji; RRID: SCR_002285
Coloc2	Daniel James White, Tom Kazimiers, Ellen Dobson	https://imagej.net/Coloc_2
GraphPad Prism7	GraphPad	https://www.graphpad.com/scientific-software/prism/; RRID: SCR_002798

RESOURCE AVAILABILITY

Lead contact

Further information and requests for resources, reagents and strains should be directed to and will be fulfilled by the lead contact, Liza A. Pon (lap5@cumc.columbia.edu).

Material availability

Plasmids and yeast strains generated in this study are available from the lead contact with a completed Materials Transfer Agreement.

Data and code availability

All data reported in this paper will be shared by the lead contact upon request. This paper does not report original code. Any additional information required to reanalyze the data reported in this paper is available from the lead contact upon request.

EXPERIMENTAL MODEL AND SUBJECT DETAILS

Yeast growth conditions

All *S. cerevisiae* strains used in this study were generated in BY4741 (*MATa his3Δ0, leu2Δ0, met15Δ0 and ura3Δ0*) background from Open Biosystems (Huntsville, AL). The maintenance and manipulation of yeast cells were conducted as previously described (Sherman, 2002). Yeast cells were propagated in YPD medium [1% (w/v) yeast extract (BD, Franklin Lakes, NJ), 2% (w/v) Bacto-peptone (BD, Franklin Lakes, NJ), and 2% (w/v) dextrose (Sigma-Aldrich, St. Louis, MO)] at 30°C with vigorous shaking at 180–200 rotations per minutes (RPM). All experiments were carried out with liquid cultures grown to the mid-logarithmic phase ($O.D._{600}$ 0.1–0.3). For aging experiments using the mCAD device, yeast cells were grown in Synthetic Complete (SC) media. For imaging experiments, all strains were washed once in SC medium [0.67% (w/v) Yeast nitrogen base without amino acids and with ammonium sulfate, amino acid mix, 2% (w/v) glucose] to reduce auto-fluorescence from YPD medium. A list of yeast strains used in this study is in Table S1.

Yeast strain construction

Knockout or tagged strains were generated essentially as described (Gardner and Jaspersen, 2014). Knockout strains were generated by using homologous recombination to replace the target genes with LEU2 selectable marker cassettes. The marker cassette was PCR-amplified from pOM13 or pOM12 plasmid (Gauss et al., 2005) with 40 bp of flanking homology upstream and downstream of the target gene. PCR reactions were performed using the KAPA HiFi PCR kit. The PCR fragments were transformed into yeast cells by the lithium acetate method described in (Gietz and Woods, 2002). In brief, yeast cells were grown to the mid-logarithmic phase, and about 2×10^8 cells were aliquoted and harvested at 3,000 × g for 1 min. Cells were washed once with 0.1 M of lithium acetate, and mixed with a transformation mixture consisting of 33.33% of PEG3350, 0.1 M lithium acetate, 0.1 mg of boiled salmon sperm carrier DNA, and 50 μL of unpurified PCR product. The transformation mixture was incubated at 30°C for 30 min, and subsequently incubated at 42°C for 45 min. Transformants were selected on agar plates containing SC medium without leucine (SC-Leu) or without uracil (SC-Ura) for 2 days. Successful transformants were confirmed by sequencing the inserted region.

To visualize Mfb1p, a bright GFP variant, GFPEnvy, was fused to the C-terminal of Mfb1p by genetic manipulation. All GFPEnvy tagged strains were generated by using the lithium acetate method described above to insert a PCR product containing the GFPEnvy gene with the *SpHis5* selectable marker after the coding region of the gene of interest. The primer sets were designed to amplify PCR fragments with 40 bp of flanking homology upstream and downstream of the stop codon of the target sequence. The backbone of the PCR product was amplified from the pFA6a-link-GFPEnvy-SpHis5 plasmid (Addgene plasmid # 60782). The PCR cassette was transformed into yeast cells and selected based on the lithium acetate transformation method described above. Transformants were selected on SC medium without histidine (SC-His) plates.

The visualization of mitochondria was achieved by C-terminally fusing mCherry to a = the mitochondrial matrix protein Cit1p. The mCherry fluorophore and the *hphMX4* selectable marker was amplified from pCY3090-02 with 40 bp of flanking homology. The PCR cassette was transformed into yeast cells and selected based on the lithium acetate transformation method described above. Transformants were selected on YPD plates containing 200 μg/mL hygromycin B (Sigma-Aldrich, St. Louis, MO).

To perform ratiometric quantification of mitochondrial redox state, endogenously expressed GDPp-mito-roGFP1 followed by the *KanMX4* selectable marker was integrated into the *HO* locus. The PCR cassette was transformed into yeast cells and selected based on the lithium acetate transformation method described

above. Transformants were selected on YPD plates containing 200 μg/mL Geneticin (Sigma-Aldrich, St. Louis, MO).

The plasmids and primers used in strain construction are listed in key resource table and Table S2.

METHOD DETAILS

Microscopy

Fluorescence microscopy was performed with one of the following imaging systems: (1) a Zeiss Axioskop 2 Plus upright fluorescence microscope with a 100×/1.4 Numerical Aperture (NA) Zeiss Plan-Apochromat objective lens (Carl Zeiss Inc., Thornwood, NY), Light-Emitting Diode (LED) module (CoolLED pE-4000, Andover, UK) and an Orca ER cooled charge-coupled device (CCD) camera (Hamamatsu Photonics, Hamamatsu City, Japan), and (2) a Zeiss AxioObserver.Z1 inverted fluorescence microscope with a 100x/1.3 oil EC Plan-Neofluar objective lens, a metal-halide lamp and an LED Colibri system (Carl Zeiss Inc., Thornwood, NY), and Orca ER cooled CCD. The first system was controlled by NIS Elements 4.60 Lambda software (Nikon, Melville, NY), and the second system was controlled by Zen Blue (Carl Zeiss Inc., Thornwood, NY). Details about the imaging conditions are given within each experimental section below.

Visualization of bud scars

To determine the age of yeast cells, bud scars were visualized by staining with Calcofluor White M2R (Millipore Sigma, Burlington, MA) or WGA conjugated to Alexa Fluor 488, 594 or 647 (Thermo Fisher Scientific, Waltham, MA). For calcofluor staining, 25 μM Calcofluor White M2R was incubated with yeast cells for 5 min, followed by 3 washes with SC media. Calcofluor-stained cells were imaged using a standard DAPI filter set (Chroma/Zeiss filter set 49; excitation G365, dichroic FT 395, emission 445/50). For WGA staining, 1 μg/mL WGA conjugated to AlexaFluor was added to a yeast cell culture and incubated for 15 min, followed by 3 washes with SC media. Alexa Fluor 488 was excited by a 470 nm LED and Alexa Fluor 594 was excited by 561 nm LED, and emission was collected with a dual eGFP/mCherry cube (#59222, Chroma, Bellows Falls, VT), or a far-red filter set (Zeiss filter set 50 HE; excitation 640/30, emission 690/50).

Enrichment of aged cells

Aged cell enrichment by binding to magnetic beads was performed as described in (Lindstrom and Gottschling, 2009; Sinclair et al., 1997; Smeal et al., 1996) with modifications. Cultures were grown overnight in YPD at 30°C to an OD_{600} < 0.2 as described above. 10^8 total cells (roughly 10 OD_{600}) of cells were harvested by centrifuging at 1500 x *g* using a Sorvall ST-16 tabletop centrifuge for 5 min. Cells were washed with 10 mL of ice-cold 1x phosphate-buffered saline (PBS) [137 mM sodium chloride, 2.7 mM potassium chloride, 10.14 mM sodium phosphate dibasic, and 1.77 mM potassium phosphate monobasic, and adjusted to pH 8]. Cells were labeled with 10 mM of EZ Link™ Sulfo-NHS-LC-LC-biotin (#21338, Thermo Fisher Scientific, Waltham, MA) dissolved in 1 x PBS for 30 min with gentle rotation at room temperature. The excessive biotin was quenched by washing cells three times with 1× PBS containing 100 mM glycine. Cells were resuspended in 1 mL of YPD and used to inoculate 500 mL of YPD media at a density of 2 × 10^5 cells/mL in a 2-L Erlenmeyer flask. Biotinylated cells were propagated at 30°C for 8 h. The OD_{600} of the culture was monitored and was not allowed to exceed 0.8. Cells were fixed by adding 20% of formaldehyde to a final concentration of 3.7% and incubated at 30°C with vigorous shaking for 50 min. Fixed cells were harvested by centrifuging at 3000 × g for 5 min, and washed with 10 mL of 1x PBS for 3 times. Cell density was measured and adjusted to 90 OD_{600} per mL, and cells were divided into 500-μL aliquots in 1.5 mL Eppendorf tubes. Miltenyi μMACs Streptavidin Micro-Beads (#130-048-101, Miltenyi Biotec Inc., Auburn, CA) were added (20 μL beads/45 OD_{600} cells) and rotated at room temperature for 30 min. Cells were washed twice with 1 mL of 1x PBS and then resuspended in 1 mL of 1× PBS. The cell suspension was sorted by MACS LS separation columns (#130-042-401, Miltenyi Biotec Inc., Auburn, CA). The separation columns were washed with 2 mL of 1x PBS and eluted with 2 mL of YPD by firmly pushing the plunger into the column. Enriched mother cells were stained with Calcofluor White as described above.

Enrichment of aged cells in the miniature-chemostat aging device and assessment of bud site selection

To determine the budding polarity in cells of different ages, aged cells were enriched in a miniature-Chemostat Aging Device (mCAD) and stained sequentially with WGA conjugated with Alexa Fluor 488 and Alexa Fluor 594. The assembly of the mCAD is described in (Hendrickson et al., 2018). In brief, cells were

grown overnight to mid-log phase (OD_{600} < 0.2). 4 OD_{600}-mL of cells were harvested by centrifuging at 1500 × g in a Sorvall ST-16 tabletop centrifuge for 5 min, and washed twice with 5 mL of 1 × PBS with 0.25% PEG3350. The cell pellet was resuspended in 0.5 mL of 1× PBS and then combined with 2 mg of EZ Link™ Sulfo-NHS-LC-LC-Biotin dissolved in 0.5 mL of 1× PBS. The biotin labeling reaction was carried out at room temperature for 30 min with gentle rotation. After the reaction, cells were washed twice with 1× PBS with 0.25% PEG3350 and then resuspended in 500 mL SC media in a 2 L Erlenmeyer flask. The biotin-labeled cells were grown at 30°C with shaking at 190–200 RPM for 8 h. The OD_{600} of the culture was monitored and was not allowed to exceed 0.3.

Labeled cells were counted using a hemocytometer. 0.9 μL of magnetic beads was used per 1 million labeled cells. Before the beading reaction, the Dynabeads MyOne Streptavidin C1 beads (#65001, Thermo Fisher Scientific) were equilibrated to room temperature and washed twice with 1 mL of SC media, and then resuspended in 20 mL of SC.

The post-biotinylated cell culture was harvested by centrifugation at 1500 × g for 5 min in a 50 mL conical-bottom tube, and the pellet was resuspended in 20 mL of SC. The concentrated cells were mixed with washed magnetic beads and rotated for 15 min at room temperature. The mother cells attached to magnetic beads were separated by ring magnets for 5 min. The supernatant was carefully removed and saved as young cells. The beaded mother cells were washed twice with 40 mL of SC, and then resuspended in 1 mL of SC media for mCAD loading.

For cell loading onto the mCAD, the vessel of the mCAD was removed from the magnets, and the air pump was set to the lowest airflow or none, and the effluent port was pulled above the media level or blocked by a tubing clamp. Beaded mother cells were transferred to a 1 mL Luer lock syringe and then loaded into the mCAD vessel by the Luer needle entry port. The loaded vessel was swirled to mix the cells, and placed on magnets to allow beaded mother cells to bind for 10 to 15 min. The media peristaltic pump (25 mL per hour) and air pump (~0.8-1 psi) were started after binding of beaded mother cells.

During mother cell harvesting, the media pump was off, and the air pump was set to the lowest setting. The effluent port was pulled up or blocked by a tubing clamp. The vessel was removed from the magnet and swirled to mix the cells. Mother cells were collected by using a Luer-lock syringe drawing from the loading port of the mCAD. The harvested cells were washed 4 times on magnets before the next procedure.

To distinguish the budding pattern in aged cells, cells were stained with WGA conjugated with 2 different AlexaFluor for visualizing the newest two bud scars on the cell surface. The staining process is described in the "visualization of bud scars" section. The mother cells were stained with WGA-Alexa488 for 15 min, washed 3 times, and diluted to OD_{600} < 0.2 in 5 mL of SC media and grown for 90 min at 30°C. Cells were then harvested and stained with WGA-Alexa594 and washed as above. Washed cells were resuspended in ~2 μL of SC and mounted on microscope slides (#3050, Thermo Fisher Scientific). Mounted cells were visualized on the microscope system 1 described above.

Analysis of mitochondrial and Mfb1p distribution

Analysis of mitochondrial distribution was performed as previously described (Pernice et al., 2016). In brief, yeast cells expressing endogenously tagged Cit1p-mCherry were imaged on System 1 or 2 using (1) a standard RFP filter set (Chroma) or (2) a Zeiss filter set 43 HE, excitation FT 570, dichroic FT 570, emission 605/70. Cells were imaged through the entire cell depth (6 μm total, with 0.3 μm z-steps), using 1 × 1 binning, 300 ms exposure with 561 nm LED with 55% power. For Mfb1p distribution, selected yeast strains expressing endogenously tagged Mfb1p-GFP or Mfb1p-GFPEnvy were imaged on System 1 or 2, with excitation by a 470 nm LED and emission collected through either (1) a dual eGFP/mCherry cube (#59222, Chroma), or (2) a Zeiss filter set 38 HE, excitation 470/40, dichroic FT 495, emission 525/50, respectively. Acquired-widefield images were deconvolved by an iterative restoration algorithm in Volocity (Quorum Technologies, ON, Canada) with a limit of 60 iterations. The relative distribution of mitochondrial mass was quantified by thresholding the mitochondrial voxels from 3D reconstructed microscopy images and calculating volume in 5 different regions (mother tip, mother center, mother neck, bud neck and bud tip, as defined in Figure 2B). The mother and bud diameters were measured along the longest axis of the cell based on the transmitted-light images. To quantify cells at similar cell cycle stages, cells were omitted if the bud-to-mother ratio was smaller than 0.2 or larger than 0.6.

Analysis of co-localization of Mfb1p and mitochondria

Co-localization between Mfb1p-GFPEnvy and mitochondria (Cit1p-mCherry) was calculated by using the Coloc2 plug-in in Fiij. Pearson's and Manders' coefficients were calculated to assess the correlation and co-occurrence, respectively, of the signals. The background of microscopic images was determined as the mean of a cell-free region near the cell of interest, and was subtracted from the image. Coloc2 was called with bisection threshold regression with a Region of Interest (ROI) flanking the cell. Coefficients and 2D intensity plots were calculated and visually inspected. Negative controls were performed by comparing a randomized channel with another channel.

Analysis of mitochondrial redox state

Analysis of mitochondrial redox state was conducted according to (Vevea et al., 2013) with modifications. The redox biosensor roGFP1 with mitochondrial targeting sequence from ATP9 was introduced into strains of interest by integration into the HO locus. Cells in mid-log phase were imaged on System 1 by excitation wavelength switching between 365 and 470 nm, and collecting emission through a modified GFP filter (Zeiss filter 46 HE without excitation filter, dichroic FT 515, emission 535/30). For the oxidized form of roGFP, a 300-ms exposure with 50% LED power was used, and for the reduced form a 200-ms exposure with 20% LED power. The-wide-field images were deconvolved as described above. The background was calculated by selecting a background ROI and subtracted from the image by thresholding in the Ratio function in Volocity. The reduced-to-oxidized mito-roGFP ratio was calculated by dividing the voxel intensity of the reduced (λex = 470 nm, λem = 525 nm) channel by that of the oxidized (λex = 365 nm, λem = 525 nm) channel. The resulting ratio channel was measured with exclusion of zero values. The mother and bud diameters were measured as described above, and the same cell-size criteria were used to exclude cells in different cell cycle stages.

Analysis of replicative lifespan

Replicative lifespan (RLS) measurements were performed as described previously (Erjavec et al., 2008), without alpha-factor synchronization. Briefly, frozen glycerol stocks of select strains (stored at −80°C) were streaked out on YPD plates and grown for 2 days. Single colonies were grown overnight in liquid YPD at 30°C, diluted and grown to exponential phase for 4 h in YPD at 30°C. 2 µL of the cell suspension was streaked onto a YPD plate and small-budded cells were isolated and arranged in a matrix using a micromanipulator mounted onto a dissecting microscope (Zeiss, Thornwood, NY). Upon completion of budding, mother cells were discarded; the time and number of divisions of the corresponding daughter cells were recorded until all replication ceased.

QUANTIFICATION AND STATISTICAL ANALYSIS

All quantifications were subjected to normal distribution analysis with the D'Agostino and Pearson normality test. Statistical p values for two-group comparison were conducted by a two-tailed Student's t test for parametric distributions and a Mann-Whitney test for non-parametric results. For more than two-group comparisons, p values were calculated by a one-way ANOVA with Dunnett's or Sidak's test for parametric distributions and a Kruskal-Wallis test with Dunn's post hoc test for non-parametric distributions. Results were recorded and sorted in Microsoft Excel and the statistical analyses were done in GraphPad Prism8 (GraphPad Software, San Diego, CA). Bar graphs and scatter graphs show the mean and standard error of the mean (SEM). For all statistical tests, p values are denoted as followed: ****$p < 0.0001$; ***$p < 0.001$; **$p < 0.01$; *$p < 0.05$.